Electronic Thesis and Dissertation Repository

8-20-2013 12:00 AM

Single Stage Flyback Micro-Inverter for Solar Energy Systems

Aniruddha Mukherjee, *The University of Western Ontario*

Recommended Citation

SINGLE STAGE FLYBACK MICRO-INVERTER FOR SOLAR ENERGY SYSTEMS

by

Aniruddha <u>Mukherjee</u>

Graduate Program in Engineering Science
Department of Electrical & Computer Engineering

A thesis submitted in partial fulfillment
of the requirements for the degree of
Masters of Engineering Science

The School of Graduate and Postdoctoral Studies
The University of Western Ontario
London, Ontario, Canada

ABSTRACT

Solar energy systems based on photovoltaic (PV) cells have attracted considerable interest in recent years due to their promise of clear and seemingly limitless generated energy. Solar energy systems based on micro-inverter architectures are gaining in popularity as they are less prone to shading and PV cell malfunction since each solar panel in a system has its own low power inverter.

A number of micro-inverters are single stage flyback inverters that are based on the DC-DC flyback topologies. There have been numerous papers on the topic of how to improve the efficiency of dc-dc flyback converters but as far as improving the efficiency of dc-ac flyback micro-inverter is concerned, comparatively less investigation on efficiency improvement has been performed.

A low cost technique for improving the efficiency of a basic dc-ac flyback micro-inverter is proposed in the paper. The proposed efficiency improving technique is based on a simple snubber, consisting of just a few passive elements. In the thesis, the flyback micro-inverter with the passive snubber is presented; the modes of operation of the converter are discussed as well as the design of the converter with the passive snubber. Experimental results obtained from a lab prototype are presented as well.

A second novel technique for improving the efficiency of a single stage flyback micro-inverter is also proposed. The technique is based on combining the simple passive snubber with a variable frequency control zero-voltage switching (ZVS) technique. In the thesis, the operation of the micro-inverter with both the passive snubber and the ZVS

technique is explained and the design of the converter is discussed. Experimental results

obtained from a lab prototype are presented to confirm the effectiveness of the both the

techniques.

Acknowledgement

The University of Western Ontario has been the ideal setting for the past two years of study and I would like to acknowledge the many selfless acts of faculty and staff, which have culminated into a productive and memorable university experience.

First, I would thank my supervisor, Dr. Gerry Moschopoulos. He has been an inspiration to me and has exposed me to another discipline of Electrical Engineering that will undoubtedly help shape my career. His guidance kept me on track during my studies and his advice to me was invaluable.

Part of this research was performed in the ePower Lab of Queen's University and I would like to thank my colleagues there. I am greatly obliged to Dr. Majid Pahlevaninezhad for his advice and valuable suggestions at various stages of the project. I would like to thank Dr.Pritam Das for his technical support. I would also like to thank my friends at ePOWER: Amish Servansing, Nikhil Sukesh, Suzan Eren, Matt Mascioli, Marco Christi, Chris Fiorentino, Nabil Akel, Ali Moallem, Alireza Safaee and Behnam Koushki.

Lastly, I would like to thank my Mom and Dad and my sisters Agnita and Lopamudra who helped me to grow up in a highly supportive and environmentally conscious atmosphere, and my brother-in-law Avik, who made me feel at home in a new country. I am forever indebted to my parents who have been a constant source of inspiration throughout my life.

Table of Contents

Table of Figures

Nomenclature

BCM	*Boundary Conduction Mode.*
CCM	*Continuous Conduction Mode.*
C_{clamp}	*Clamp capacitor (F).*
C_o	*Output capacitor (F).*
DCM	*discontinuous Conduction Mode.*
d	*Duty cycle.*
d_l	*duty cycle of a particular switching period.*
d_{pk}	*Peak duty cycle in AC cycle.*
f_{sw}	*Switching frequency(Hz).*
i_l	*Primary switch current (A).*
I_{l_pk}	*Peak primary switch current (A).*
i_{do}	*Secondary diode current (A).*
i_{in}	*Input current (A).*
I_{in_avg}	*Average input current (A).*
I_o	*Output current (A).*
i_{tr}	*Auxiliary winding current (A).*
L_m	*Magnetizing inductance (H).*
L_{lk}	*Leakage inductance of the transformer (H).*
L_o	*Output inductor (H)*
N	*Turns ratio.*
N_p	*Primary number of turns.*
N_s	*Secondary number of turns.*
N_{tr}	*Auxiliary number of turns.*
N_r	*Auxiliary turns ratio.*
P_{in}	*Input power (W).*
P_o	*Output power (W).*
PWM	*Pulse width modulation.*
T_{on}	*Primary switch on time (s).*
T_{off}	*Primary switch off time (s).*

T_{do}	Secondary diode conduction time (s).
T_{qr}	Time period of the resonant cycle (s).
T_{grid}	Time period of the 60Hz AC (s).
V_{in}	Input voltage (V).
V_o	Output voltage(V).
v_{ds}	Voltage across the primary switch(V).
v_{clamp}	Voltage across the clamp capacitor(V).
v_{clamp_max}	Maximum voltage across the clamp capacitor (V).
v_{clamp_min}	Minimum voltage across the clamp capacitor (V).
v_{tr}	Voltage across auxiliary winding (V).
Δv_{clamp}	Change in capacitor voltage (V).
v_r	Reflected instantaneous voltage at start of resonance (V).
v_x	Drop in reflected voltage (V).
ZCS	Zero current Switching.
ZVS	Zero voltage switching.

Chapter 1

1   Introduction

Renewable sources of energy are becoming more popular due to environmental concerns and the need for more energy. The use of renewable energy was 1684 million tons of oil equivalent (Mtoe) in 2010, accounting for 13% of global primary energy demand.[1] Electricity generation from wind grew by 27% and solar photovoltaics (PV) by 42% per year on average during this period [1, 2]. Current forecasts such what is shown in Figure 1-1 predict that solar energy systems in particular will grow exponentially in the future.
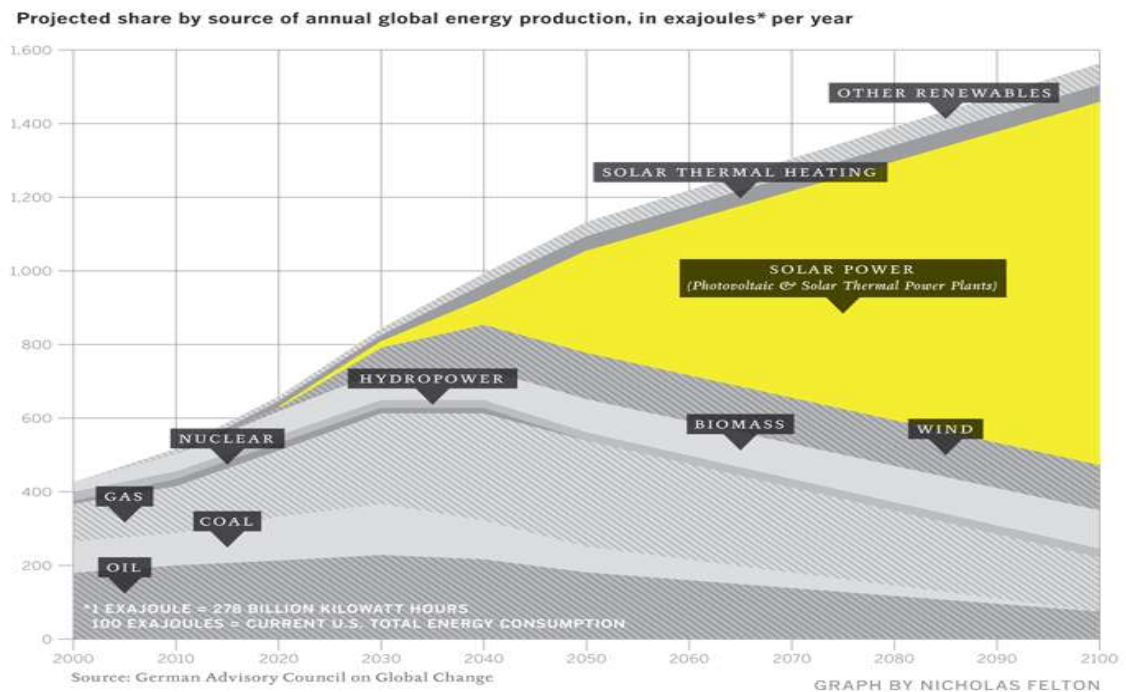
Figure 1-1 Projection of global energy production. [2]

Inverters, which are DC-AC power electronic converters, are an important component of any PV system. These PV inverters are part of the power conversion infrastructure that converts the power available from PV panels to AC that can be fed to the grid. There are three general types of inverter architectures: central inverters, string inverters, and micro-inverters [3-8]. Each architecture has its own merits and demerits and is shown in Figure 1-2.

Central inverter architecture is the standard choice for high-power PV systems because it is the simplest and cheapest option as just a few inverters are used with many PV modules. Typically, the central inverter system has comparatively better or equal efficiency than the other architectures, but it misses maximum power point operation for each module due to shading and clouding effects which decreases the overall efficiency of the system.

String inverters represent a compromise between central and microinverters. A string inverter is used for just one string of modules (8 to 10 solar panels) so that multiple string inverters are connected together to form a larger systems. Although small number of inverters are required for a large PV system but it also suffers from the shading and clouding effects. Therefore, efficiency of the overall system is low.

In micro-inverter architectures, each solar panel has its own inverter that performs power conversion for each module. Micro-inverter architectures are more expensive than the other two, but offer the highest power optimization and design flexibility and also avoid a single point of failure. The main focus of this thesis is on micro-inverters, particularly micro-inverters that are based on the flyback converter topology.
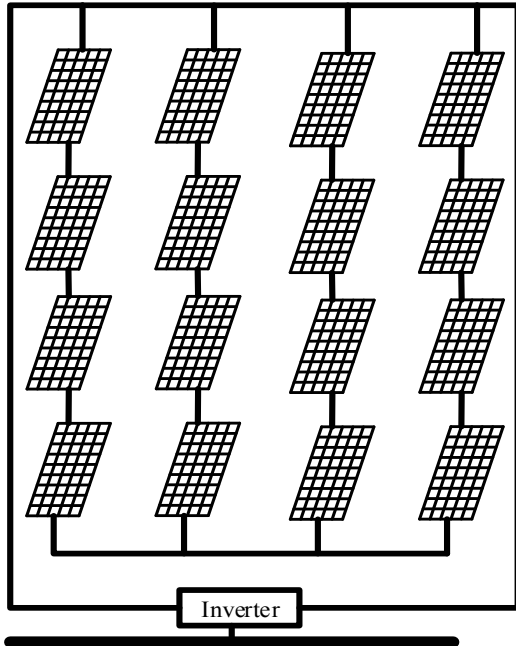
(a) Central inverter
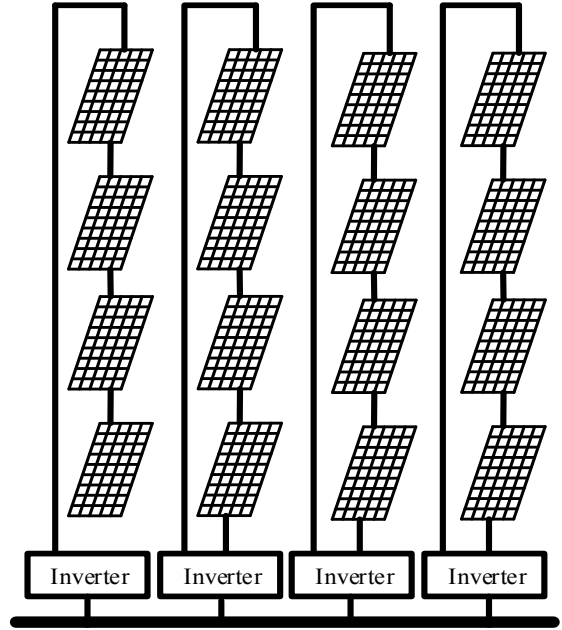
(b) String Inverter
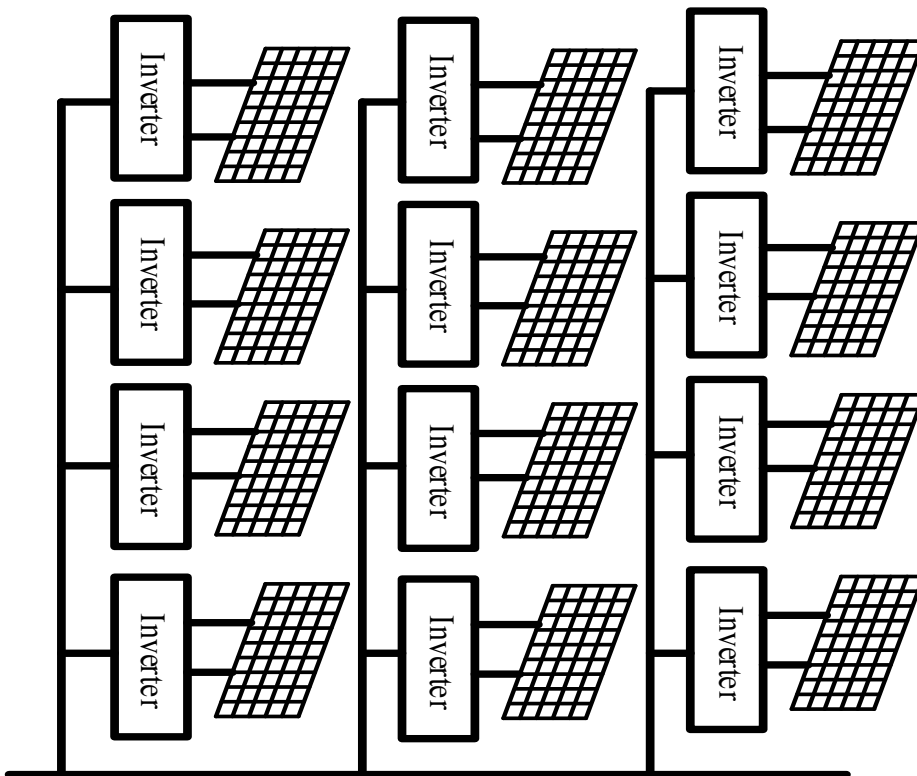
(c) Microinverters

Figure 1-2 Inverter architectures.

1.1 Literature review

In this section the state of the art in the field of single-stage flyback micro-inverters are discussed. The general principles behind flyback micro-inverters [9-13] are reviewed and several previously proposed flyback micro-inverters are presented with their advantages and disadvantages discussed.

1.1.1 Conventional flyback inverter

The conventional flyback micro-inverter is shown in Figure 1-3. The way this converter works is as follows: When the primary switch, S_1, is on, the full input DC voltage from the PV panel is impressed across the transformer, thus putting energy into its magnetizing inductance and making its magnetizing current rise. When S_1 is turned off, the energy that was stored in the transformer's magnetizing inductance is transferred to the output, which is the grid. Since the output is AC, this means that it is either transferred through D_{o1} and S_{o1} when the output voltage is positive or through D_{o2} and S_{o2} when it is negative.

The duty cycle of S_1 must be made to vary throughout the AC voltage line cycle so that it is at its minimum when the AC voltage is at its minimum and it is at its maximum when the AC voltage is at its peak. As a result, the converter must be implemented with some control scheme that can track the AC grid voltage and synchronize its operation to this voltage.

Figure 1-4 shows typical waveforms for the flyback inverter. It can be seen that, as the gate pulse of switch S_1 becomes high at $t=T_2$ and the switch is turned on, the switch current, i_{s1}, rises and the voltage (v_{ds}) across the switch S_1 becomes zero. At T_2, the switch

is turned off, the current i_{s1} cannot go to zero suddenly because inductance l_{lk} in the current path. Also the secondary diodes take some time to turn on, for the period T_2-T_3 there will be some voltage spike. At T_3 the secondary diodes conduct and the stored energy in the transformer is transferred to the load. During this period there will be an additional reflected voltage across the main switch on top of input voltage. As the secondary current goes to zero at T_4 there is no reflected voltage, hence the v_{ds} will be same as V_{in}.
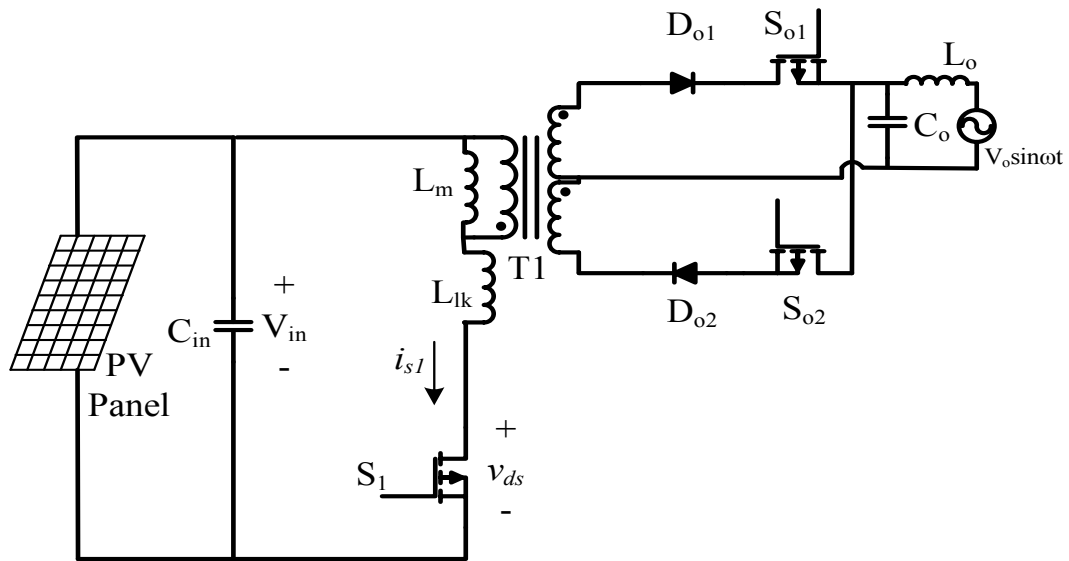
Figure 1-3 Conventional flyback inverter
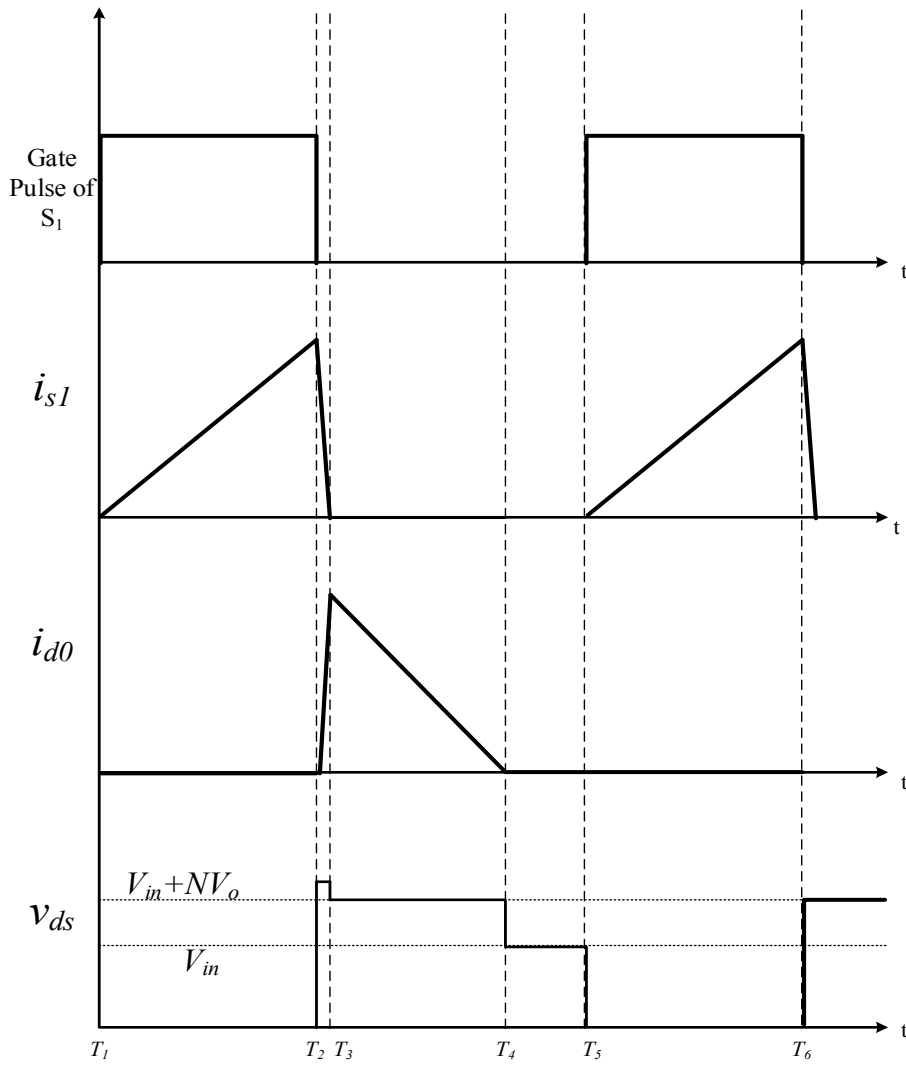
Figure 1-4 Typical operating waveform of a flyback converter.

1.1.2 Flyback inverter operated in different conduction modes

The flyback micro-inverter can be operated with its magnetizing current in continuous conduction mode (CCM), discontinuous conduction mode (DCM), or boundary conduction mode (BCM) [9, 10]. When the converter is operated in CCM with

continuous magnetizing current (Figure 1-5), the primary peak current is lower than that when the converter is operating in DCM or BCM so that converter turn-off losses are lower as well. The control of the output current, however, is difficult as the converter has a right-hand plane (RHP) zero in its transfer function when it is operated in CCM. As a result, the converter needs to be implemented with a complex control scheme to avoid having a distorted output current, which makes CCM operation unsuitable for low cost PV micro-inverters [12, 13].

Discontinuous conduction mode (DCM) operation is preferred for flyback micro-inverters [9-11], which is shown in the Figure 1-6. When a flyback micro-inverter is operated in DCM, its transformer is completely discharged by the end of each switching cycle and its current is a train of triangular pulses whose peaks are bounded by a sinusoidal reference envelope.

These current peaks, however, can be high; one way to reduce these current peaks is to operate the converter in BCM (Figure 1-7). With BCM, S_1 is turned on as soon as the magnetizing current falls to zero, after the transformer has been fully demagnetized, so that this current is at the boundary of CCM and DCM. The main drawback with BCM, however, is that the converter must be operated with variable frequency control as the length of the switching cycle must vary throughout the AC grid voltage line cycle. As a result, the control scheme required to implement the converter in BCM is more sophisticated than what is required for DCM, but it is not as sophisticated as what is required for CCM. Moreover, the switching frequency may become very high for certain applications especially when the converter must operate over a wide input voltage range

and load range and this can create switching losses that can reduce the converter efficiency.

As a result, some authors have proposed the use of hybrid schemes (i.e.combination of DCM and BCM) where the converter is made to operate with a combination of DCM and BCM, depending on the operating conditions. For example, the converter is designed to operate with a certain maximum frequency with BCM; as the load is decreased, then so too is the switching frequency. For lighter loads, when the switching frequency can become so low that it enters the audible range, the converter is made to operate with DCM with a fixed switching frequency that is just above this range.
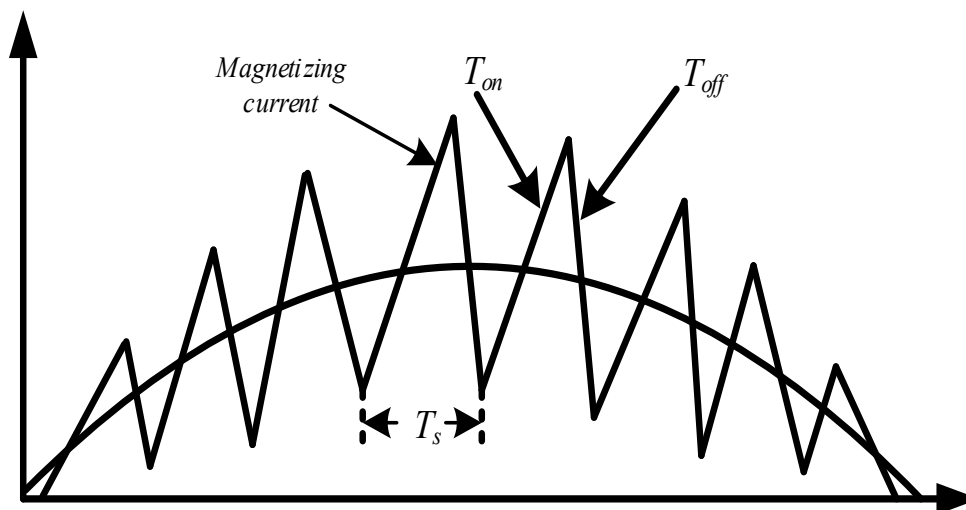
Figure 1-5 Continuous conduction mode of magnetizing current.
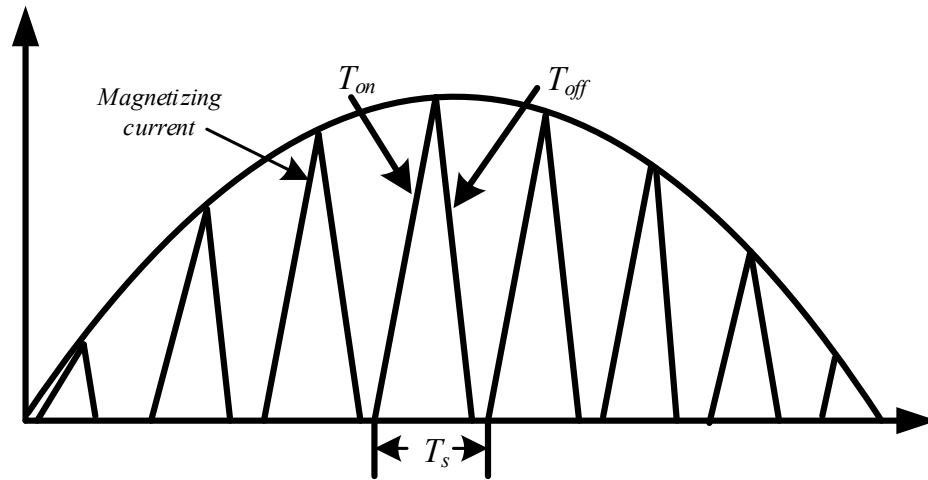
Figure 1-6 Discontinuous conduction mode of magnetizing current.
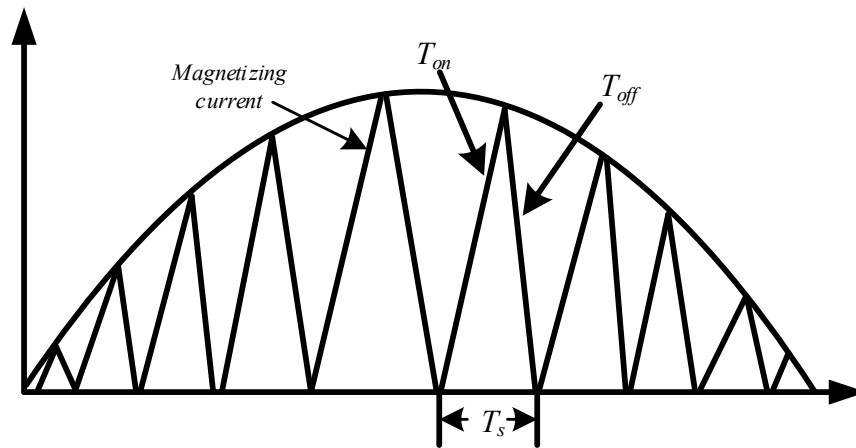
Figure 1-7 Boundary conduction mode of magnetizing current.

1.1.3 Flyback microinverters in PV power system

A flyback inverter is one of the common topologies considered for PV modules since it

provides a simple circuit configuration to achieve direct conversion of the DC power to

AC power. The flyback topology has proved to provide a reliable and cost effective topology with reduced number of semiconductor switches.

A number of variations on the conventional flyback micro-inverters shown in Figure 11-16, which are typically operated either in DCM or BCM, have been proposed in the literature. In this section, several of these variations are reviewed.

1.1.4 Active clamp flyback inverter

One variation on the conventional flyback micro-inverter is the addition of an active clamp that allows its primary switch, S_1, to operate with zero-voltage switching ZVS [14-18]. Although S_1 in the conventional converter can be turned on with zero-current switching (ZCS) when the inverter is operated in either DCM or BCM as there is no primary current when the switch is turned on (thus having fewer turn-on losses than with CCM operation, but more turn-off losses), the energy that is stored in its parasitic juction capacitance of the main switch is dissipated in the switch when it is turned on. Consequently, ZVS is preferred for high switching frequency applications to avoid this energy loss.

An example of an active clamp flyback inverter is shown in Figure 1-8. The inverter is operated in the same manner as the conventional inverter except that the auxiliary switch, S_a, is turned on just before S_1 is turned on. What this action does is that it injects negative resonant current into the transformer that is used to discharge the parasitic MOSFET capacitance of S_1. As the parasitic capacitance of S_1 is completely discharged, thus the voltage across the switch becomes zero and the anti-parallel diode turns on, allowing S_1 to turn on with ZVS.

The ability of S_1 to turn on with ZVS is dependent on the amount of energy that is available is discharge its parasitic junction capacitance. When the output AC voltage is near its zero crossing point, the converter's duty cycle is at its mini-mum and so the amount of current in its primary. As a result, there may not be sufficient energy available to completely discharge the output capacitance of S_1 so that S_1 cannot turn on with full ZVS. The converter must be implemented with a more sophisticated topology or control scheme if it is desired to ensure that S_1 can turn on with ZVS throughout the full AC line cycle.
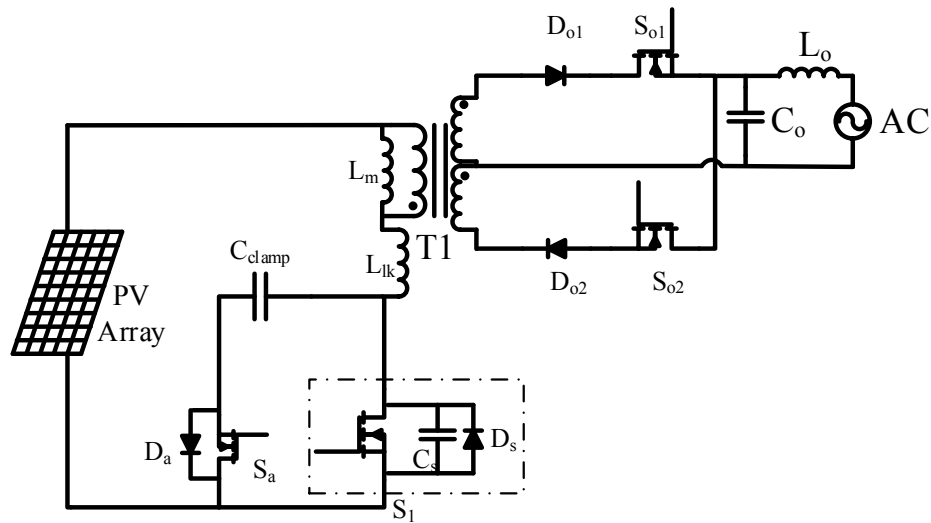
Figure 1-8 Active clamp flyback microinverter

1.1.5 ZVS using grid current

An example of how the ZVS operation of the primary switch of a flyback inverter can be extended is shown in Figure 1-9 [19]. In this topology, there is no primary side auxiliary circuit or active clamp, but the diodes that were at the secondary (D_{o1} and D_{o2} in Figure 1-3 and 1-8) have been replaced by active switches. This is to make the secondary branches to be bidirectional so that current can flow out of the grid as well as into the grid.

The basic principle behind this converter is to use current from the grid to assist the ZVS turn-on of S_1. This can be done in the following manner: When S_1 is off and the transformer is demagnetizing, the magnetizing current (and thus the secondary current) drops. If this current is allowed to drop to zero, current will start to flow in the opposite direction, out of the grid and into the converter. This secondary current causes a current to appear in the converter's primary that can be used to discharge the parasitic MOSFET capacitance of S_1 so that it can be turned on with ZVS.

Since this current can be generated during most of the AC grid voltage line cycle whether it is at its peak or close to a zero-crossing point the ZVS turn-on of S_1 can be ensured throughout most of the line cycle. This feature, however, comes at the cost of a more sophisticated control scheme as variable switching frequency control is needed to limit the secondary current and care must be taken to ensure that the current that is drawn from the grid, which does not contribute to power but only to conduction losses, does not offset the gain in efficiency that is achieved by the ZVS of S_1.
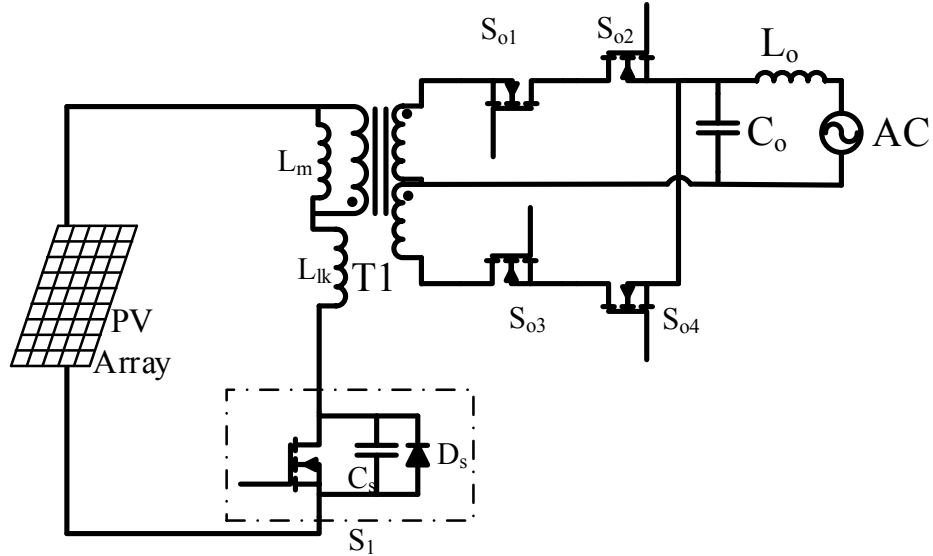
Figure 1-9 ZVS flyback inverter using grid current

1.1.6 Flyback inverter with switched capacitor turn-off snubber

In addition to turn-on losses, the primary switch of a flyback inverter can have turn off losses. This is especially true when it is considered that the input voltage of flyback microinverters is typically low and they are made to operate in DCM, so that the current that this switch has to turn off can be considerable. For some applications, it may be that it is the turn-off losses and not the turn-on losses that are dominant as the turn-on losses can be low when the input voltage is low.

The turn-off losses in the primary switch can be reduced if the switch is implemented with some sort of turn-off snubber. One such approach was proposed in [20] and is shown in Figure 1-10. Although, the converter in Figure 1-10 was proposed for a higher power inverter (1 kW), it can be used in lower power, high current applications. In this converter, the primary switch of the conventional converter is replaced with a circuit structure that consists of two switches, S_1 and S_2, two diodes, D_1 and D_2, and a snubber

capacitor C_{clamp}. C_{clamp} is charged by energy from the transformer leakage inductance through D_1 and D_2 during the latter part of each switching cycle.

The converter works in the same way as the conventional inverter except that the two switches are turned on at the same time. When this happens, the full primary current initially flows through both S_1 and S_2 and C_{clamp}. If C_{clamp} is fully discharged, which may not be the case if the primary current is very low, the primary current then splits, with half the current flowing through S_1 and D_2 and the other half flowing through D_1 and S_2. After some time has passed, both S_1 and S_2 are turned off simultaneously with ZVS as the rise in voltage across both switches is limited by C_{clamp}.
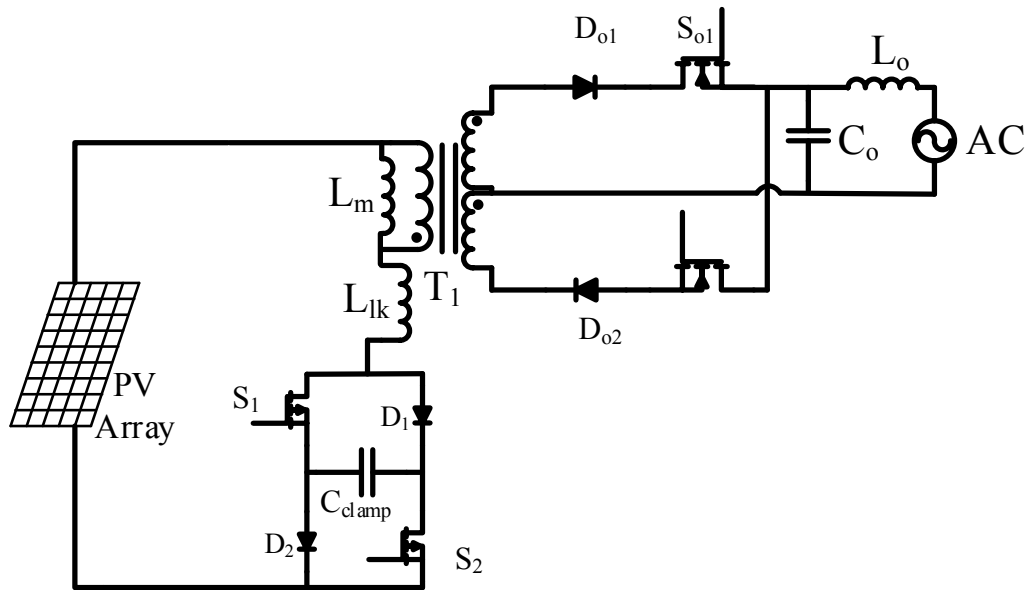
Figure 1-10 Flyback inverter with switch capacitor snubber

With respect to the ZVS active clamp inverter discussed in Section 1.1.4, the inverter shown in Figure 1-10 has one additional diode. This inverter can be considered as an

option for low input voltage, high current applications while the active clamp inverter should be considered for higher input voltage, lower current applications.

1.1.7 Interleaved flyback inverters

Microinverters can be implemented using a single converter, as has been demonstrated so far in this paper, or using multiple interleaved converters [21-31]. Examples of interleaved converters for PV applications are shown in Fig. 2(d)-(f).

When interleaved converters are used, the secondary switches are not placed in series with the secondary diodes of each flyback converter; instead there is a separate, low frequency converter that is used to interface the output of the flyback converters to the grid voltage. When the grid voltage is positive, a diagonally opposed pair of inverter switches is on throughout the half cycle; when the voltage is negative, the other pair is on.

Although a microinverter can be implemented in various ways, flyback converters are attractive because of their simplicity and low cost. Their operation, however, is generally restricted to < 200 W so that if a microinverter is implemented with a flyback converter, then an interleaved arrangement such as what is shown in Figures 1-11,12,13 needs to be used. The cost of having two converters can be justified for higher power applications in a way that cannot be for lower power applications where a single flyback inverter is preferred.

The basic principle of interleaved flyback converters is that multiple converters or "phases" are connected in parallel so that each converter phase is interleaved with the others. If two converter phases are used, then each one is operated 180° out of phase with

respect to the other (i.e. the primary switch of each converter has the same gating signal as that of the other, but shifted by 180° in the switching cycle).

Each converter can be operated in the same way as the converters described above. Figure 1-11 shows an interleaved arrangement consisting of two conventional flyback converters; Figure 1-12 shows and interleaved arrangement consisting of two active clamp flyback converters [21]; Figure 1-13 shows an interleaved arrangement consisting of two conventional flyback converters, but with a turn-off snubber that allows some of the energy that would other-wise be dissipated in the turn-off process to be fed back into the converter [23]. The converters for each phase can be operated using CCM, DCM, or BCM, whichever mode is preferred.
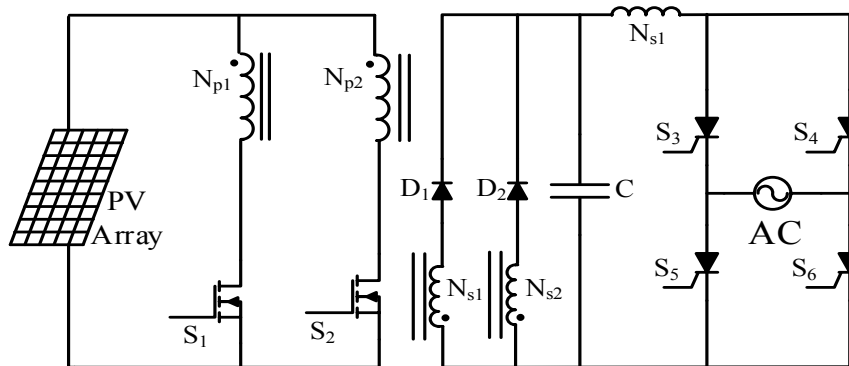
Figure 1-11 Interleaved flyback inverter
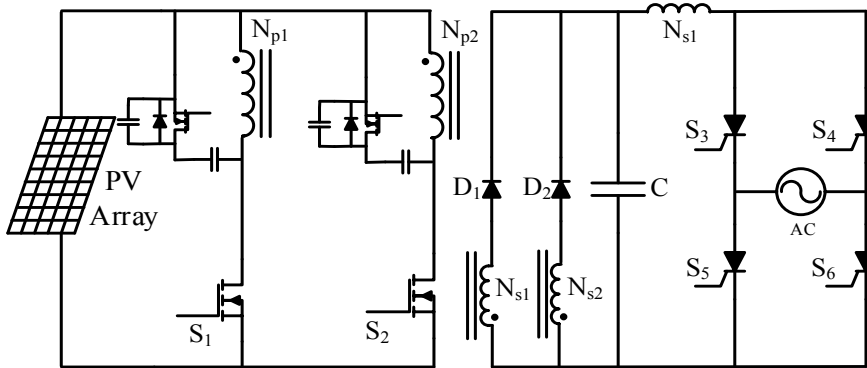
Figure 1-12 Active clamp interleaved flyback inverter
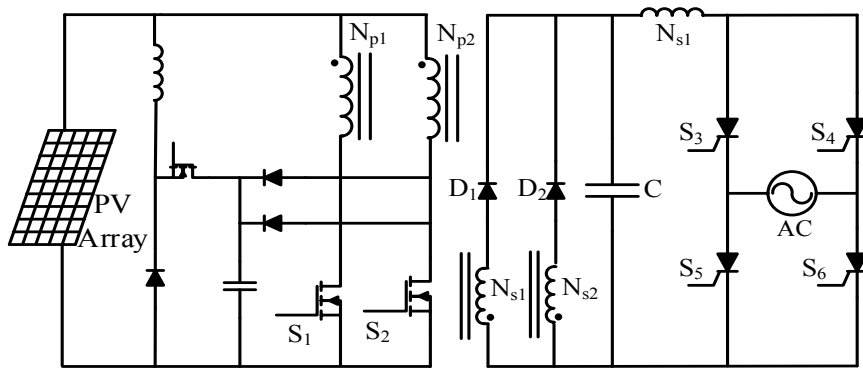
Figure 1-13 ZVS Interleaved flyback inverter

1.2 Thesis Objectives

The main objectives of this thesis are as follows:

- To propose new flyback micro-inverters with improved converter efficiency that does not require the use of active auxiliary circuits.

- To develop a design procedure for each new converter that can be used in the selection of critical converter components

- To confirm the feasibility of each new converter with experimental results obtained

from proof-of-concept prototype converters.

1.3 Thesis Outline

In addition to this chapter, this thesis comprised of three other chapters. The outline of the remainder of this thesis is as follows:

In Chapter 2, a new flyback micro-inverter with a passive regenerative energy snubber that reduces the turn-off losses of the primary switch is proposed. The principles behind the snubber are discussed, the operation of the new converter is explained and its modes of operation are presented. The design of the converter is discussed and simulation and experimental results from a lab prototype are presented to show the effectiveness of the snubber in improving converter efficiency.

In Chapter 3, another flyback micro-inverter is proposed. The converter is similar to the converter proposed in Chapter 2, but it is made to operate with ZVS using quasi-resonant circuit principles. As a result, both the turn-on losses and the turn-off losses of the primary switch can be reduced. The modes of operation of the converter are discussed and design of the converter is explained in the chapter. Simulation and experimental results obtained are presented to confirm the effective of the new dual soft-switching technique.

In Chapter 4, the contents of the thesis are summarized, the conclusions that have been reached as a result of the work performed in thesis are presented, and the main contributions of the thesis are stated. The chapter concludes by suggesting potential future research that can be done based on the thesis work.

It should be noted that the main focus of this thesis is on the new flyback micro-inverter topology with the regenerative snubber and with the ZVS technique. The control methods that are used to operate the converter are based on the work presented in [15, 16, 19, 26-35] and are not discussed as they are considered to be outside the scope of this thesis.

Chapter 2

2   Proposed Flyback Micro-Inverter with Energy Regenerative Snubber

It was explained in the previous chapter that flyback micro-inverters have switching losses that are mainly caused by the turning on and off of their main primary switch (typically a MOSFET). Such switching losses are due to the power loss that is related to the product of the voltage across a switch device and the current flowing through it during a switching transition. Several methods that use auxiliary circuits to reduce these losses were presented in Chapter 1. Some of these methods use an additional active switch to help discharge the output capacitance of the primary switch before it is turned on so that it can do so with zero-voltage switching (ZVS); without such methods, the energy stored in the output capacitance would be dissipated in the MOSFET.

Flyback micro-inverters are typically exposed to low input DC voltages (i.e. around 40 V). As a result, turn-on losses are not as significant as they are in higher voltage applications as less energy is stored in the switch output capacitance. Moreover, even though they are low power converters, the current that flows through their transformer primary side (input side) can be high. This is especially true when it is considered that flyback micro-inverters are designed to operate so that their transformer is fully demagnetized before the end of each switch cycle, which results in high peak currents. Turning off the primary-side switch in such inverters, with such peak currents, results in turn-off losses that can be significant [36-43].

These turn-off losses can be reduced if the primary-side switch is implemented with some sort of snubber that slows down the rate of voltage rise across the switch when it is turning off, thus reducing the switch voltage-current product. The term "snubber" is derived from the fact that it also helps to "snub" voltage spikes that can appear across a switch when current flow is interrupted with the turning off of the device. Typically, a turn-off snubber has a capacitor that appears across the switch when it is turning off. This snubber capacitor is larger than the output capacitance of the switch device and adds to the total capacitance across the switch; the more capacitance that appears across the switch, the slower the switch voltage rise during turn off will be.

Using a passive snubber to reduce turn-off losses can result in efficiency gains, without the need for more sophisticated ZVS techniques that use an active switch in their auxiliary circuits. A key drawback with many turn-off snubbers, however, is the fact that they dissipate energy. Energy that is stored in the snubber capacitor after the switch has been turned off is then wasted sometime later during the switching cycle.

A flyback micro-inverter with a passive regenerative energy turn-off snubber is proposed. The main feature of this converter is that efficiency gains can be achieved using a very simple passive snubber that does not waste all the energy that is placed in it during a switching cycle. In the chapter, the new micro-inverter is introduced, its operation is explained in detail and a design procedure based on mathematical analysis is developed.

The procedure is demonstrated with a design example and the feasibility of the proposed converter is confirmed with results obtained from a prototype converter.

2.1   Converter Operation

The proposed flyback micro-inverter is shown in Figure 2-1. Its transformer primary side is like a dc-dc flyback converter with S_1 being the main power switch. Attached to the primary side are a passive snubber circuit consisting of diodes D_1 and D_2, capacitor C_{clamp} and transformer winding T_r, which is a winding that is taken from the main power transformer so that the snubber circuit actually results in the addition of only three components: D_1, D_2, C_{clamp}.
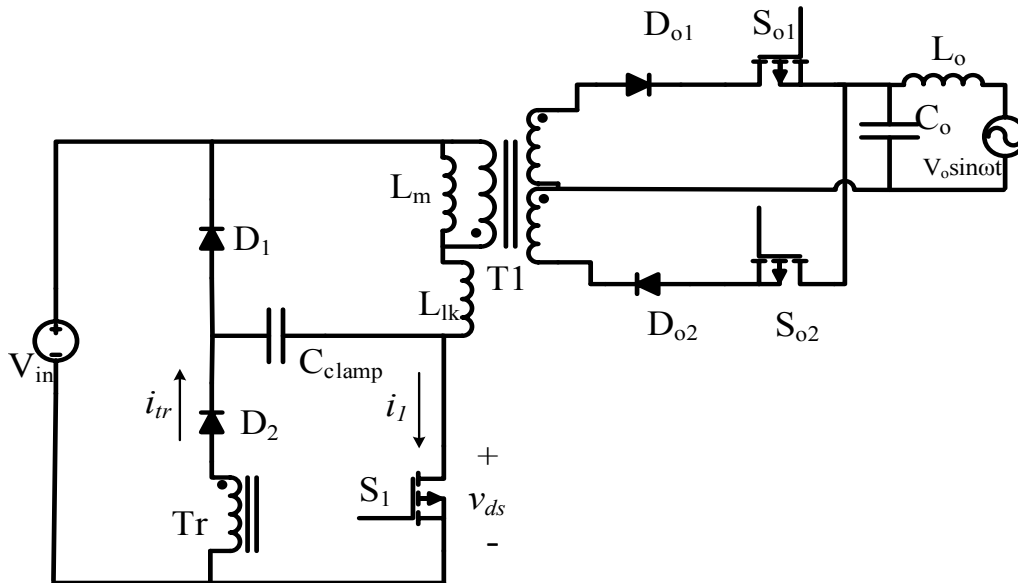
Figure 2-1 Proposed flyback microinverter with passive snubber.
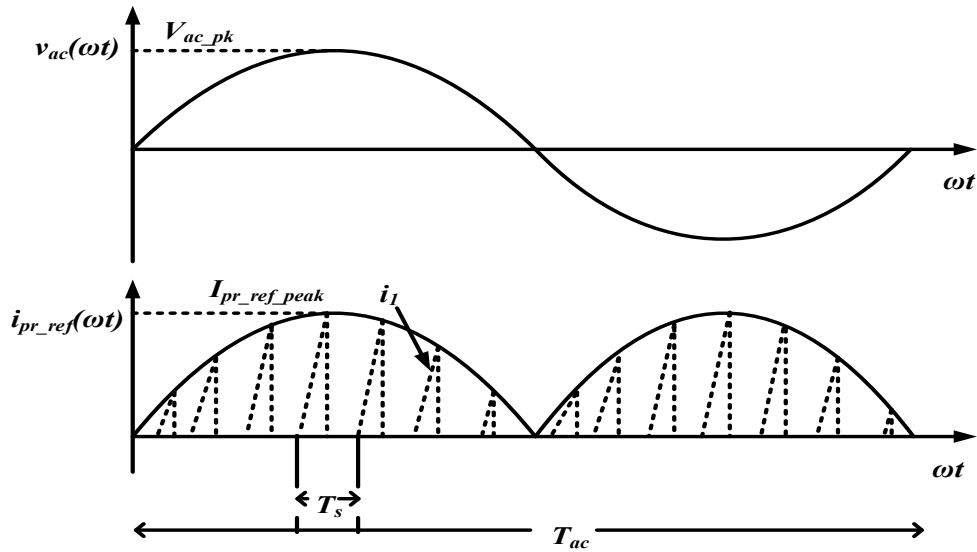
Figure 2-2 Waveform for 60 Hz AC cycle.

The basic principle that must be followed to ensure that the microinverter produces an appropriate ac output waveform is that the flyback transformer must be fully demagnetized before the start of the next switching cycle. If the converter's duty cycle is made to vary throughout the ac line cycle (small duty cycle for the zero crossing regions of the ac waveform, larger duty cycle for the peak regions) then a discontinuous ac current waveform can be produced at the secondary. The secondary side switches S_{o1} and S_{o2} are turned on and off in an appropriate manner to ensure an AC output waveform synchronized with the grid. S_{o1} is on and S_{o2} is off if it is needed for energy to be transferred to the ac output with a positive polarity and S_{o1} is off and S_{o2} is on if it is needed for energy to be delivered to the output with a negative polarity. The output capacitor can filter the output produced by the rest of the converter so that the appropriate final output is produced and fed to the grid.

The flyback micro-inverter goes through several modes of operation during a switching cycle. Typical waveforms for a switching cycle are shown in Figure 2-4 and equivalent circuit diagrams that show the flow of current during any particular mode of operation are shown in Figure 2-3. The inverter's modes of operation are as follows:

Mode 1 – [T0-T1] (Figure2- 3(a)):

The switching cycle begins with the turning on of primary side switch S_1 at $t = T_0$. When this happens, the source voltage is impressed across the main transformer primary winding and the transformer magnetizing inductance starts to energize. At the same time, as the switch S_1 is turned on, the diode D_2 turns on as well. Therefore, the charged (as a result of the previous switching cycle) clamp capacitor C_{clamp} discharges through the switch S_1 and the auxiliary winding T_r. This mode concludes as the diode D_2 turns off.

Mode 2 – [T1-T2] (Figure2- 3(b)):

As a result of the previous mode, capacitor C_{clamp} has been discharged to such an extent that at $t = T_1$, the voltage across C_{clamp} is such that diode D_2 is reverse biased. Therefore, the transformer continues to be magnetized, but only due to the voltage impressed across the main transformer winding.

Mode 3 – [T2-T3] (Figure2- 3(c)):

The primary side switch S_1 is turned off at $t = T_2$. As a result, current no longer flows through S_1, but flows through two paths instead one is through the output capacitance of S_1, C_s, and the other is through C_{clamp} and diode D_1, after the voltage across C_s reaches a voltage of $V_{in} + NV_o + v_{clamp}$ (where V_{in} is the input source voltage, V_o is the absolute

24
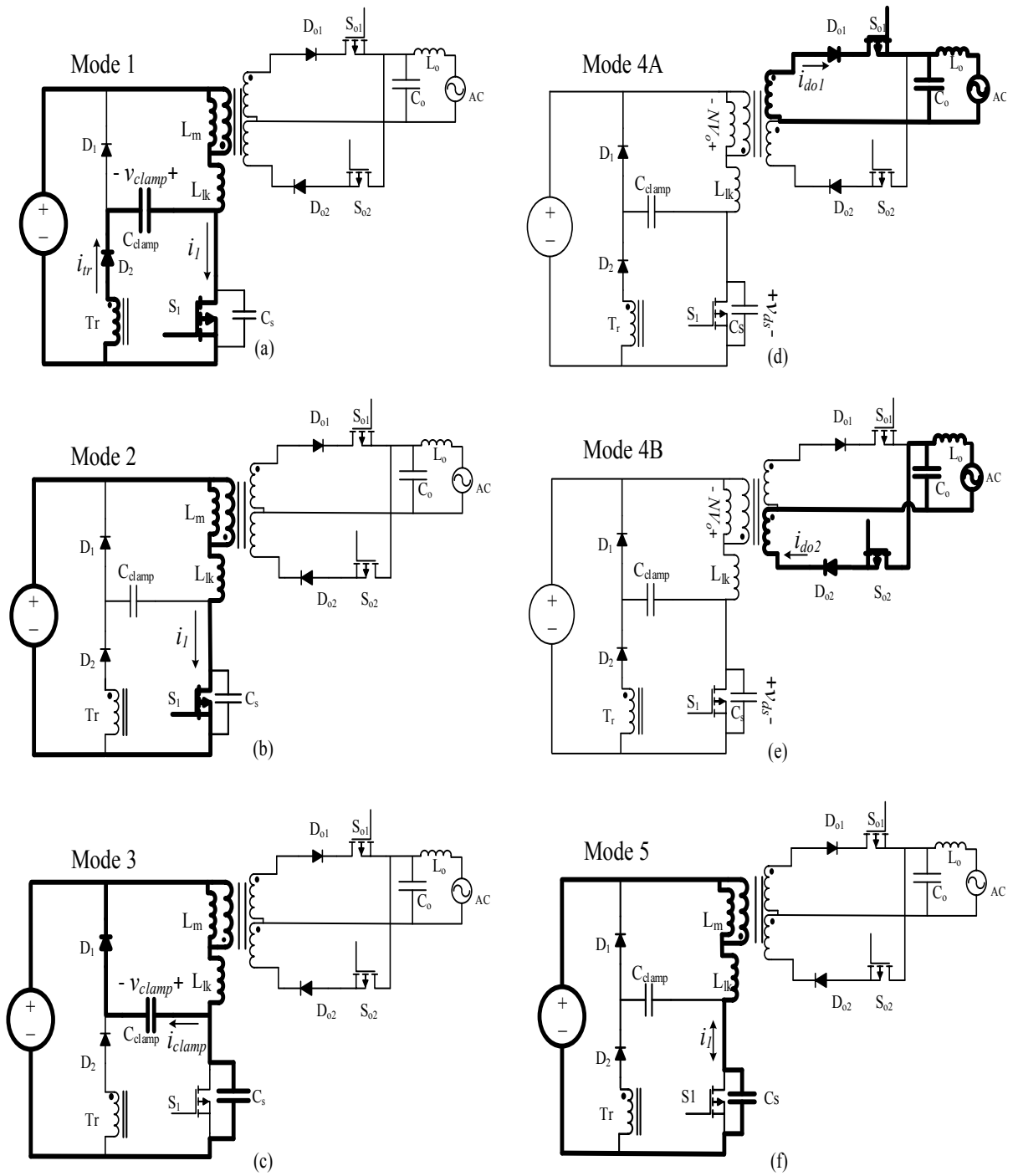
Figure 2-3 Modes of operation (Note: Mode 4 is divided into (d) and (e) depending on the polarity of the 60 Hz AC sine wave.

value of the instantaneous ac output voltage and N is the turns ratio of the main transformer winding N_p/N_s). By the end of this mode, the voltage across C_{clamp} reaches its maximum value.

Mode 4 –[T3-T4] (Figure2- 3(d)):

At $t = T_3$, the transformer begins to be demagnetized as one of the secondary diodes begins to conduct. The diode that conducts depends on the polarity of the output AC voltage. If this voltage is positive, then S_{o1} is on and current flows through D_{o1} (Figure 2-3(d)); if this voltage is negative, then S_{o2} is on and current flows through D_{o2} (Figure 2-3(e)). This mode ends when the secondary current goes to zero at T4.

Mode 5 –[T4-T5] (Figure2- 3(f)):

After the secondary current goes to zero, there is no reflected voltage across the transformer primary. As a result, the magnetizing inductance begins to resonate with the output capacitance of the switch, C_s. This resonance between the switch parasitic capacitor and magnetizing inductance causes the voltage across the switch to swing between $V_{in} \pm NV_0$ to Depending on the duty cycle a part, complete, or multiple resonant cycles can occur during this period. This mode ends when switch S_1 is turned on to start the next switching cycle.
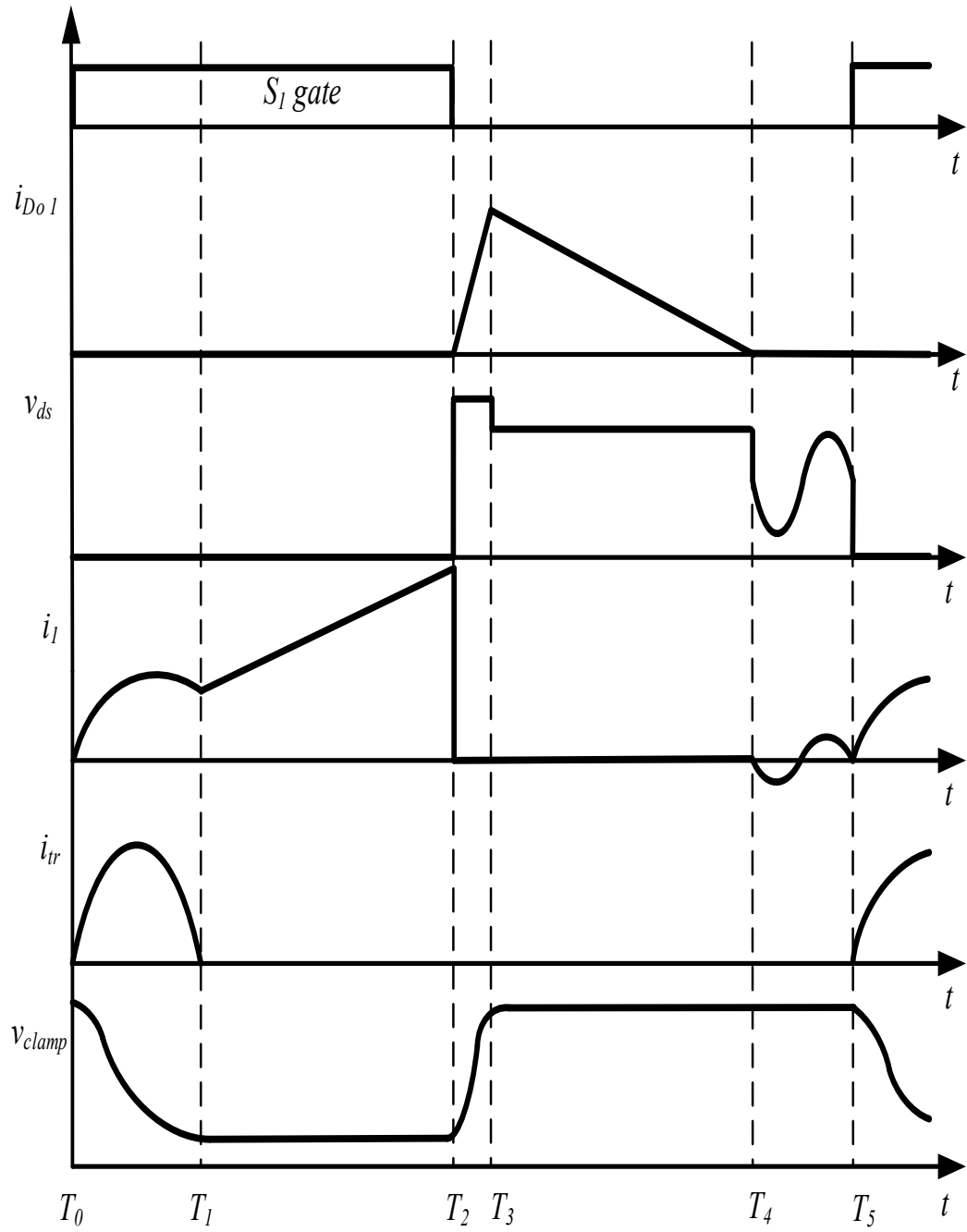
Figure 2-4 Typical converter waveforms.

2.2   Converter features

The proposed micro-inverter has the following attractive features:

- The passive snubber that is attached to the primary side of the converter is very simple and requires only a few passive components. Such a simple approach is satisfactory since the input voltage is low according to standard practice for the input of a micro-inverter attached to a solar panel and thus the dominant switching losses are turn-off losses.

- Some of the energy that would otherwise be trapped in C_{clamp} and dissipated in resistor is recovered through the auxiliary transformer winding T_r, thus resulting in improved efficiency. Moreover, the transfer of this energy is done seamlessly, along with the energy stored through the main transformer winding, so that the output voltage is not distorted as a result of the energy transferred from the auxiliary winding.

2.3   Converter Design

The design of the proposed converter can be split into two parts. For the first part, the focus is on the design of the main converter, without considering the snubber; for the second part, the focus is on the design of the regenerative snubber itself. The design of each part is discussed in detail in this section of the thesis.

A. Main Converter Design

The following are the most important considerations when it comes to the design of the main converter:

- As discussed in the Introduction section of this chapter, it is imperative that the micro-inverter be made to operate in DCM so that a sinusoidal output can be

achieved. The most important component that needs to be considered for DCM operation to be ensured is the magnetizing inductance L_m of the transformer. If a value of L_m is chosen to be too low, then the peak primary current will have higher peaks that will increase the current stress placed on switch S_1 and will force this switch to turn off with a large amount of current flowing through it. If the value of L_m is chosen to be too high, then the current through it may move toward continuous conduction mode and thus it may not be possible to produce an appropriate output voltage.

- The selection of L_m and the selection of N are interrelated as one parameter is dependent on the other. In this section, it is assumed that a value of N has been previously determined as a starting point for the design and it is shown how a value of L_m can be subsequently determined. The selection of N is discussed in detail in the next section of the chapter, which demonstrates how the converter can be design with a design example.

- If the converter is to be designed so that its magnetizing inductance operates in DCM, then sufficient time must be allowed within each switching cycle for the magnetizing current to fall to zero from its peak value, after S_1 has been turned off. The worst case situation occurs when the converter operates at maximum duty cycle (ratio of switch on-time t_{on} to switching cycle time T_s) d_{pk} and the primary current i_1 reaches its maximum value of $i_{pr\_ref\_pk}$ during the total grid AC cycle, as shown in Figure 2-2. This can be expressed as

$$t_{off\_pk} \leq T_s - t_{on\_pk}. \tag{2.1}$$

Where t_{off_pk} is the off time of S_1 in the switching cycle when the primary current reaches its peak value of $i_{pr\_ref\_pk}$ and t_{on_pk} is the on-time of S_1 during the same switching cycle and can be expressed as

$$t_{on\_pk} = d_{pk}T_s = d_{pk}\frac{1}{f_s} \tag{2.2}$$

Where f_s is switching frequency.

The current in L_m can drop to zero when S_1 is turned off and the energy that is stored in it is transferred to the output. When S_1 is turned off, the voltage across the transformer is the output voltage that appears across the secondary winding and is reflected to the primary. This voltage can be expressed as

$$v_{grid} = V_{grid\_pk} \sin \omega_g t \tag{2.3}$$

Where V_{grid_pk} is the peak value of output voltage and ω_g is the grid frequency. Considering this voltage reflected to the primary, the fall of current in L_m can be expressed as

$$Nv_{grid}(t) = L_m \frac{di_1(t)}{dt} \tag{2.4}$$

So that t_{off} can be expressed as

$$t_{off\_pk} = L_m \frac{I_{1\_pk}(t)}{NV_{grid\_pk}} \tag{2.5}$$

To determine the turn off-time t_{off_pk}, the peak primary current flowing through the flyback inverter I_{1_pk} needs to be determined. This can be done by considering the fact that the

input dc voltage V_{in} is impressed on the transformer primary when S_1 is on, as shown for Mode 2 in Figure. 2-3(b). The rise in current when S_1 is on can be expressed as

$$V_{in} = L_m \frac{di_1(t)}{dt} \qquad (2.6)$$

Substituting equation (2.2) into this equation gives the following expression for I_{1_pk}:

$$I_{1\_pk} = \frac{V_{in}d_{pk}}{L_m f_s} \qquad (2.7)$$

Substituting this equation into equation (2.5) gives,

$$t_{off\_pk} = \frac{V_{in}d_{pk}}{V_{grid\_pk}f_s N} \qquad (2.8)$$

It can be seen from equation (2.8) that t_{off_pk} is dependent on various parameters. Assuming a fixed switching frequency f_s, these parameters are fixed except for peak duty cycle d_{pk} and turns ratio N. Values for d_{pk} and N need to be chosen so that the converter remains in DCM. This can be done by considering the expression for DCM operation given in equation (2.1) and substituting equation (2.8) into this equation to get

$$\frac{V_{in}d_{pk}}{V_{grid\_pk}f_s N} \leq T_s - t_{on\_pk} \qquad (2.9)$$

If both sides of this equation are divided by $t_{on\text{-}pk}$, then

$$\frac{V_{in}}{V_{grid\_pk}N} \leq \left(\frac{1}{d_{pk}} - 1\right) \qquad (2.10)$$

Which can be either be rearranged to give the following equation for turns ratio:

$$N \geq \frac{V_{in}}{V_{grid\_pk}} \left(\frac{1}{d_{pk}} - 1 \right)^{-1}$$ (2.11)

or rearranged to give the following expression for peak duty cycle:

$$d_{pk} \leq \frac{1}{\frac{V_{in}}{NV_{grid\_pk}} + 1}$$ (2.12)

With expressions for DCM operation derived, the next step is to determine an appropriate value of magnetizing inductance L_m that can store sufficient energy to be fed to the grid, for a rated output power P_o. Once this has been determined, the final step is to confirm that the converter can operate with DCM with this value of L_m, using the DCM expressions that have been derived.

If the converter is assumed to be ideal and lossless, then the input power P_{in} can be expressed as

$$P_{in} = P_o$$ (2.13)

Since the input voltage source is dc, therefore the input power is dependent on the average current that flows out of this source I_{in_avg} so that

$$P_{in} = V_{in} * I_{in\_avg}$$ (2.14)

Since $I_{in,avg}$ is dependent on L_m, therefore finding an expression that relates $I_{in,avg}$ to L_m will achieve the objective of finding a relation between L_m and P_o.

The first step in determining $I_{in,avg}$ is to integrate the primary current $i_1(t)$ over a period, according to the standard definition of averaging. Since the period of the primary current

is half that of the line cycle T_{grid}, as can be seen from Figure 2-2, this integration can be expressed as

$$I_{in\_avg} = \frac{1}{T_{grid}/2} \int_0^{T_{grid}/2} i_1(t) dt \qquad (2.15)$$

The primary current is the summation of a triangular pulses so that

$$I_{in\_avg} = \frac{1}{T_{grid}/2} \sum_{i=1}^n \int_0^{t_{on}} i_1(t) dt \qquad (2.16)$$

Where $i=1, 2, 3...n$ and n is the number of switching cycles per half ac line cycle so that,

$$nT_s = \frac{T_{grid}}{2} \qquad (2.17)$$

From equation (2.17) n can be written as

$$\frac{T_{grid}/2}{T_s} = n \qquad (2.18)$$

The integration of one of these triangular pulses for an ith switching cycle can be expressed as

$$\int_0^{t_{on}} i_1(t) dt = \int_0^{t_{on}} \frac{V_{in}t}{L_m} dt \qquad (2.19)$$

The on-time of S_1 for the switching cycle when the primary current is at its peak value was defined in equation (2.2) to be

$$t_{on\_pk} = d_{pk} T_s = d_{pk} \frac{1}{f_s} \qquad (2.20)$$

33

Since the current peaks of the peak current follow a sinusoidal envelope, the converter's duty cycle can be expressed in terms of a sinusoidal so that

$$t_{on} = T_s d_{pk} \sin \omega_g t; \qquad \omega_g t \in [0, \pi] \qquad (2.21)$$

From the description of equation (2.17), $\sin \omega_g t$ can be written as $\sin \omega_{gi} T_s$, when $i=1,2,3..n$. Using the definition of $\omega_g t$ in equation (2.21), the following relation can be written:

$$\sin \omega_g t = \sin \frac{\pi}{\frac{T_{grid}}{2}} i T_s \qquad (2.22)$$

From equation (2.18) this can be expressed as,

$$\sin \omega_g t = \sin \frac{\pi}{n} i \qquad (2.23)$$

Hence, using equation (2.21) t_{on} can be expressed as

$$t_{on} = T_s d_{pk} \sin \left(\frac{\pi}{n} i \right) \qquad (2.24)$$

Substituting this equation in equation (2.19) gives

$$\int_0^{t_{on}} \frac{V_{in} t}{L_m} dt = \frac{V_{in}}{2L_m} T_s^2 d_{pk}^2 \left(\sin \left(\frac{\pi}{n} i \right) \right)^2 \qquad (2.25)$$

If equations (2.16) and (2.25) are combined, then the following expression can be obtained for the average current:

$$I_{in\_avg} = \frac{V_{in} T_s^2 d_{pk}^2}{T_{grid} L_m} \sum_{i=1}^{n} \left(\sin \left(\frac{\pi}{n} i \right) \right)^2 \qquad (2.26)$$

Equation (2.26) can be expressed as,

$$I_{in\_avg} = \frac{V_{in}T_s{}^2 d_{pk}{}^2}{T_{grid}L_m} \sum_{i=1}^{n} \left(\sin\left(\frac{\pi}{n}i\right)\right)^2 \tag{2.27}$$

Equation (2.27) can be further simplified by multiplying both numerator and denominator with n so that

$$I_{in\_avg} = \frac{V_{in}nT_s{}^2 d_{pk}{}^2}{T_{grid}L_m} \frac{1}{n}\sum_{i=1}^{n} \left(\sin\left(\frac{\pi}{n}i\right)\right)^2 \tag{2.28}$$

The term $\frac{1}{n}\sum_{i=1}^{n} \sin(\frac{\pi}{n}i)^2$ can be expressed as

$$\frac{1}{n}\sum_{i=1}^{n} \sin(\frac{\pi}{n}i)^2 = \frac{1}{n}\sum_{i=1}^{n} \frac{1}{2}\left[1 - \cos\left(\frac{2\pi}{n}i\right)\right] \tag{2.29}$$

$$= \frac{1}{2} - \frac{1}{2n}\sum_{i=1}^{n} \cos\left(\frac{2\pi}{n}i\right) \tag{2.30}$$

By using the sum of cosine formula [51] $\sum_{n=1}^{n} \cos(nx) = \frac{\sin\left[\left(n+\frac{1}{2}\right)x\right] - \sin(x/2)}{2\sin(x/2)}$ equation (2.30) can be written as

$$\frac{1}{2} - \frac{1}{2n}\sum_{i=1}^{n} \cos\left(\frac{2\pi}{n}i\right) = \frac{1}{2} - \frac{1}{2n}\left[\frac{\sin\left[\left(n+\frac{1}{2}\right)\frac{2\pi}{n}\right] - \sin\left(\frac{\pi}{n}\right)}{2\sin\left(\frac{\pi}{n}\right)}\right] \tag{2.31}$$

This expression can be further simplified to be

$$\frac{1}{2} - \frac{1}{2n}\left[\frac{\sin\left[\left(n+\frac{1}{2}\right)\frac{2\pi}{n}\right] - \sin\left(\frac{\pi}{n}\right)}{2\sin\left(\frac{\pi}{n}\right)}\right] = \frac{1}{2} - \frac{1}{4n}\left[\frac{\sin\left(2\pi+\frac{\pi}{n}\right)}{\sin\left(\frac{\pi}{n}\right)} - 1\right] \tag{2.32}$$

$$= \frac{1}{2} - \frac{1}{4n}\left[\frac{\sin\left(\frac{\pi}{n}\right)}{\sin\left(\frac{\pi}{n}\right)} - 1\right] = \frac{1}{2} \tag{2.33}$$

Therefore equation (2.29) is can be written as,

$$\frac{1}{n}\sum_{i=1}^{n}\sin(\frac{\pi}{n}i)^2 = \frac{1}{2} \qquad (2.34)$$

By replacing $\frac{1}{n}\sum_{i=1}^{n}\sin(\frac{\pi}{n}i)^2$ with 1/2, the average current in equation (2.28) can be written as

$$I_{in\_avg} = \frac{V_{in}nT_s{}^2d_{pk}{}^2}{2T_{grid}L_m} \qquad (2.35)$$

Substituting the value of T_{grid} from equation (2.18) in equation (2.35) results in

$$I_{in\_avg} = \frac{V_{in}T_s d_{pk}{}^2}{4L_m} \qquad (2.36)$$

Which can rewritten in terms of switching frequency as

$$I_{in\_avg} = \frac{V_{in}d_{pk}{}^2}{4f_sL_m} \qquad (2.37)$$

Substituting thus equation into equations (2.13) and (2.14) gives

$$\frac{V_{in}{}^2d_{pk}{}^2}{4f_sL_m} = P_{in} = P_{out} \qquad (2.38)$$

In this equation, power is given in terms of input voltage of input voltage. Flyback micro-inverters normally supply the grid, so that the power expression in equation (2.38) can be represented in terms of grid RMS voltage.

The RMS value of the grid voltage is given by,

$$V_{grid\_rms} = \frac{V_{grid\_pk}}{\sqrt{2}} \qquad (2.39)$$

Substituting this voltage in equation (2.39) and rearranging it gives

$$P_o = \frac{V_{in}{}^2 d_{pk}{}^2 V_{grid\_rms}{}^2}{4 f_s L_m \left(\frac{V_{grid\_pk}}{\sqrt{2}}\right)^2} \tag{2.40}$$

Which can be written as,

$$P_o = \frac{1}{2}\left(\frac{V_{in}}{V_{grid\_pk}}\right)^2 \frac{d_{pk}{}^2 V_{grid\_rms}{}^2}{f_s L_m} \tag{2.41}$$

If this equation is rearranged, then the relation between magnetizing inductance L_m and power can be established to be

$$L_m = \frac{1}{2}\left(\frac{V_{in}}{V_{grid\_pk}}\right)^2 \frac{d_{pk}{}^2 V_{grid\_rms}{}^2}{f_s P_o} \tag{2.42}$$

And thus the objective of determining such a relation has been achieved. It will be shown in the design example how this power equation and the DCM equations (2.11) and (2.12) can be used to design the main converter.

2.3.1   Design of the regenerative snubber

The passive regenerative snubber consists of an auxiliary winding that is taken from the main power transformer, two diodes and capacitor C_{clamp}. Without the snubber, the energy in the leakage inductance that has accumulated just before S_1 is turned off would be transferred to the output capacitance of the switch. Since this capacitance (C_s) is small, this would result in a voltage spike appearing across the switch that would damage it. The clamp capacitor (C_{clamp}) of the snubber circuit absorbs the leakage energy and reduces the voltage spike. The snubber should be designed so that the voltage spike is not excessive.

The value of the clamp capacitor can be determined by considering the energy balance between clamp capacitor C_{clamp} and the transformer leakage inductance as almost all of the leakage energy is eventually transferred to the clamp capacitor. This energy balance can be expressed as

$$\frac{1}{2}C_{clamp}\delta v_{clamp}{}^2 = \frac{1}{2}L_{lk}I_{1\_pk}{}^2 \tag{2.43}$$

The maximum voltage rise across the snubber capacitor (δv_{clamp}) can be determined by rearranging equation (2.43) to give

$$I_{1\_pk} \times \sqrt{\frac{L_{lk}}{C_{clamp}}} = \delta v_{clamp} \tag{2.44}$$

If the allowable voltage rise limits are predetermined then, the value of the clamp capacitor can be determined by,

$$C_{clamp} = \frac{L_{lk}I_{1\_pk}{}^2}{\left(\delta v_{clamp}\right)^2} \tag{2.45}$$

C_{clamp} cannot be too large because if it is, then it may not be possible to allow for sufficient time for it to discharge and thus the voltage across it will accumulate. This discharge time is dependent on the values of C_{clamp} and L_{lk}, the transformer leakage inductance and can be expressed as:

$$C_{clamp < \frac{1}{L_{lk}}\left(\frac{T_{on}N_p}{\pi N_{tr}}\right)^2} \tag{2.46}$$

To design the auxiliary winding, the equivalent circuit of Mode 1 in Figure 2-3(a) needs to be considered. From this figure, it can be determined that the resonant cycle can only continue until the capacitor voltage remains higher than the auxiliary winding voltage. As

the switch S_1 is on during this period, the voltage across the auxiliary winding is the reflected primary winding voltage. The auxiliary winding voltage is given by

$$v_{tr} = V_{in} \frac{N_{tr}}{N_P} \qquad (2.47)$$

Where N_{tr} is the number of auxiliary turns and N_r ($N_r = \frac{N_{tr}}{N_P}$ is auxiliary winding turns ratio

so that

$$v_{clamp\_max}(t) > V_{in}N_r \qquad (2.48)$$

2.3.2   Converter Design Example

A design example that shows how the converter can be designed is presented in this section. For the example, the converter is to be design for input voltage V_{in} = 40-50 Vdc V_o = 110 V AC, maximum output power $P_{o.max}$ = 100W, grid voltage frequency 60Hz and switching frequency f_s = 100 kHz, which is a typical frequency used for this application. The transformer leakage inductance is $L_{lk} = 0.4\mu H$. It should be noted that the design procedure is iterative and that several iteration must be done before a satisfactory design can be achieved. What is shown in this section is the final iteration.

A. Duty cycle and turns ratio selection

To determine the peak duty cycle, it needs to be ensured that the converter remains in DCM and that the transformer is effectively utilized (meaning that it should not operate with extremely high or extremely low duty cycles if it can be avoided). To achieve the peak grid voltage from minimum 40 V input voltage, a graph of peak duty cycle and turns ratio can be plotted by using equation (2.12), as shown in Figure 2-5.
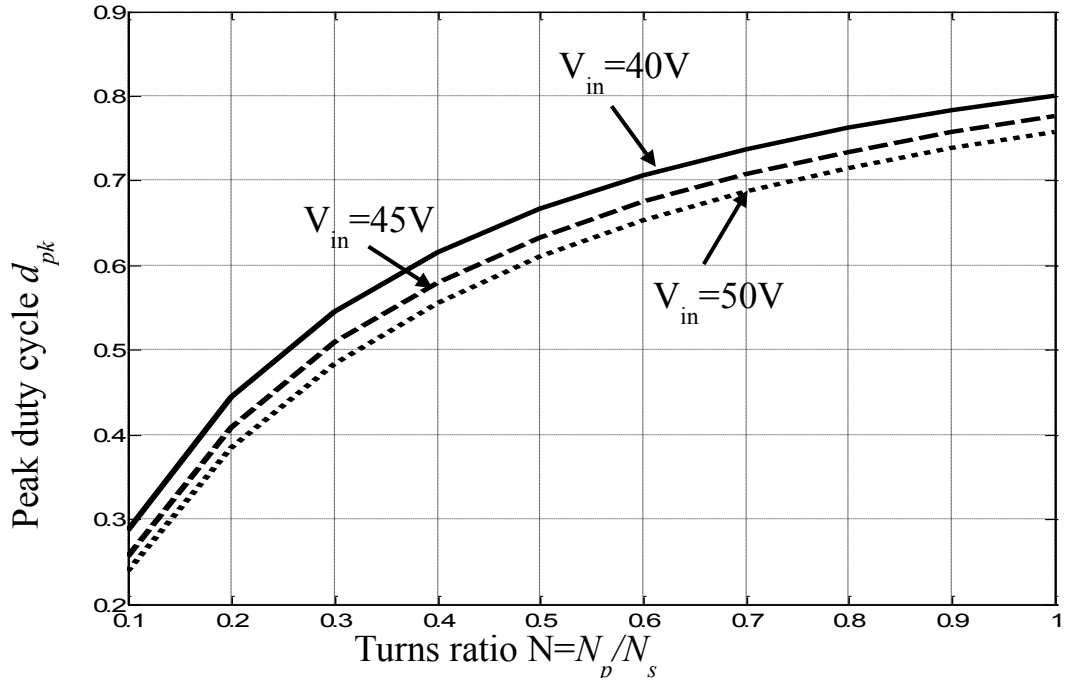
Figure 2-5 Required peak duty cycle and turns ration for different input voltage.

From Figure 2-5, it can be seen that within the range d_{pk}=0.4 to d_{pk}=0.6, a transformer turns ratio ranging from 0.2 to about 0.4-0.5 can be considered. For DCM operation, the total conduction time should be less than time period, which is 10μs for 100 kHz switching frequency. From equation (2.8), the total conduction time can be expressed as

$$t_{on} + t_{off} = d_{pk}t_s\left[1 + \left(\frac{V_{in}}{V_{grid\_pk}N}\right)\right] \qquad (2.49)$$

Figure 2-14 can be drawn. From this figure, it can be determined that a peak duty cycle of d_{pk}=0.55 can be used for DCM operation so that the turns ratio can be determined using equation (2.11) to be,

$$\frac{V_{in}}{V_{grid\_pk}}\left(\frac{1}{d_{pk}} - 1\right)^{-1} \le N = 0.32 \qquad (2.50)$$
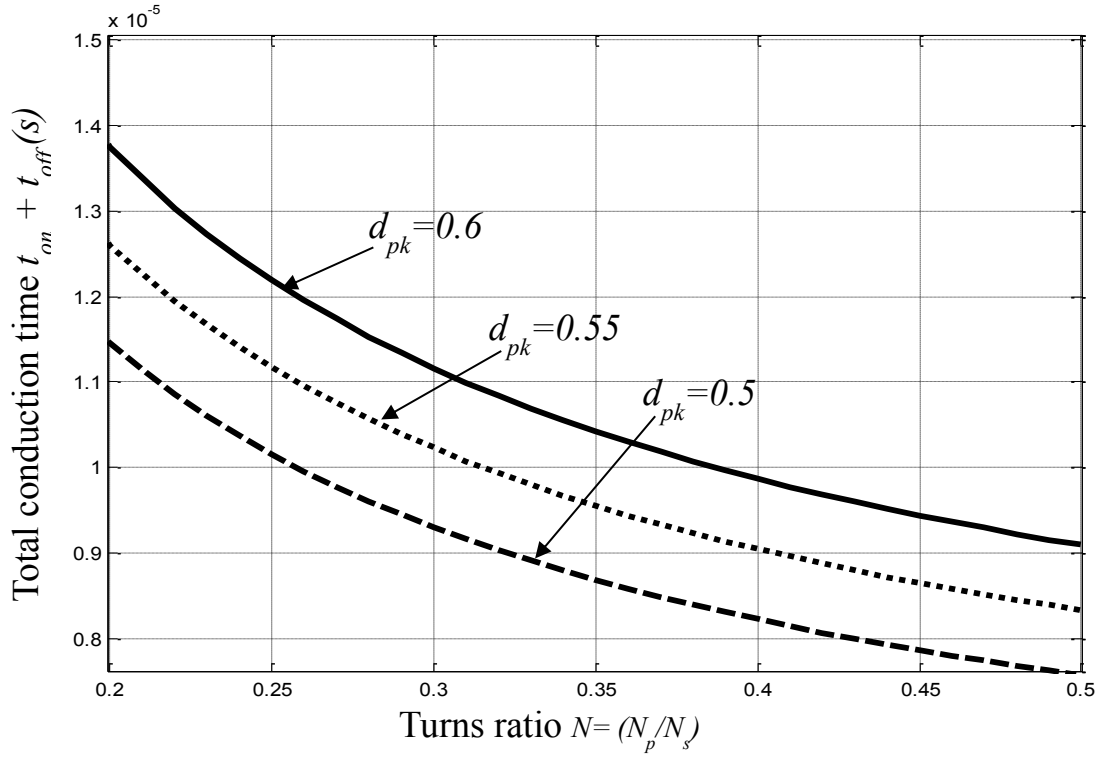
Figure 2-6 Variation of conduction time with turns ratio and duty cycle.

B. Magnetizing Inductance (L_m)

A value for the magnetizing inductance can be found using equation (2.42). Substituting

V_{in} = 40, $V_{grid,pk}$ = 155µH, d_{pk} = 0.55, into equation (2.42) gives

$$L_m = \frac{1}{2}\left(\frac{V_{in}}{V_{grid\_pk}}\right)^2 \frac{d_{pk}{}^2 V_{grid\_rms}{}^2}{f_s P_o} = \frac{1}{2}\left(\frac{40V}{155V}\right)^2 \frac{(0.55)^2(110V)^2}{(100\ kHz)(100\ W)} = 12.8\mu H \qquad (2.51)$$

C. Clamp capacitor value

An appropriate value for the clamp capacitor can be determined using equation (2.45) in

Section 2.3.1 If a Δv_{clamp} = 25V (50% of peak input voltage as standard) and a leakage

inductance of $L_{lk} = 0.4\mu H$ are considered (based on previous iterations) and a value of $I_{1\text{-}pk} = 20A$ is considered as well, then the value of the capacitor can be determine to be

$$C_{clamp} = \left(\frac{I_{1\_pk}}{\Delta v_{clamp}}\right)^2 \times L_{lk} = \left(\frac{20}{25}\right)^2 \times 0.4 \times 10^{-6} \cong 0.25\mu F. \qquad (2.52)$$

D. Auxiliary Winding turns ratio

To design the auxiliary turn's ratio maximum voltage across the capacitor need to be considered as the auxiliary circuit turns on during the clamp capacitor voltage at its maximum value. Maximum voltage across the clamp capacitor can be found from the previous section and equation (2.44), which is given by,

$$v_{clamp\_max} = NV_0 + \Delta v_{clamp} \qquad (2.53)$$

From equation (2.48) it was found that

$$V_{in}N_r < v_{clamp\_max} \qquad (2.54)$$

Considering the above condition, diode D_2 needs to be turned off during the secondary diodes conducting. Therefore this relation can be written as,

$$V_{in} + NV_0 > v_{clamp\_min} + v_{tr} \qquad (2.55)$$

As the minimum voltage across the capacitor is the reflected secondary voltage this can be written as

$$V_{in} > N_r V_{in} \qquad (2.56)$$

Therefore, $N_r < 1$ according to equation (2.56). By decreasing N_r impedance of the resonant circuit decreases therefore the peak resonant current increases significantly. If the auxiliary turns ratio is higher, this resonant discharge will take longer time as the resonant frequency decreases. Considering the above conditions auxiliary turns ratio is selected $N_r=0.78$

2.4   Simulation Results

The feasibility of the proposed converter was tested using PSIM software, a commercially available power electronics simulation software package. The converter was implemented with the following specifications: V_{in} = 40-50V, Vo =110VAC, f_s=100 kHz and P_{o_max} =100W. It was implemented with the component values found from the design sections. The determined component values are given in Table 1.

Table 1

Turns Ratio (N)	0.32
Magnetizing Inductance (L_m)	12.8μH
Leakage Inductance (L_{lk})	0.4 μH
Clamp Capacitor (C_{clamp})	250nF
Auxiliary Turns Ratio(N_r)	0.78

Simulation results are presented in Figures 2-8, 2-10. In these figures, i_1 is the primary switch current, v_{ds} is the voltage across the primary switch S_1, i_{do1} is the current flowing through the secondary diode and I_o is the output current.

Figure 2-8 shows the primary switch gating signal and the current that flows through it. It can be seen that the current is a triangular waveform as the converter operates in DCM. It can also be seen that there is hump in the switch current just after the gate pulse becomes high and the switch is turned on. This is due to the current that flows through the auxiliary winding. Because of integration of the auxiliary winding with the main transformer, the leakage energy stored in the capacitor is transferred to the output

In Figure 2-9, it can be seen that the voltage across the switch S_1 reaches its peak as the switch is turned off and this voltage is clamped by the clamp capacitor. After the capacitor gets charged, the secondary current ramps up and energy stored in the magnetizing inductance is delivered to the load.

Figure 2-10 shows the primary current and the output load current. It can be seen that both currents are sinusoidal waveforms, with the switch current being a rectified sinusoid.
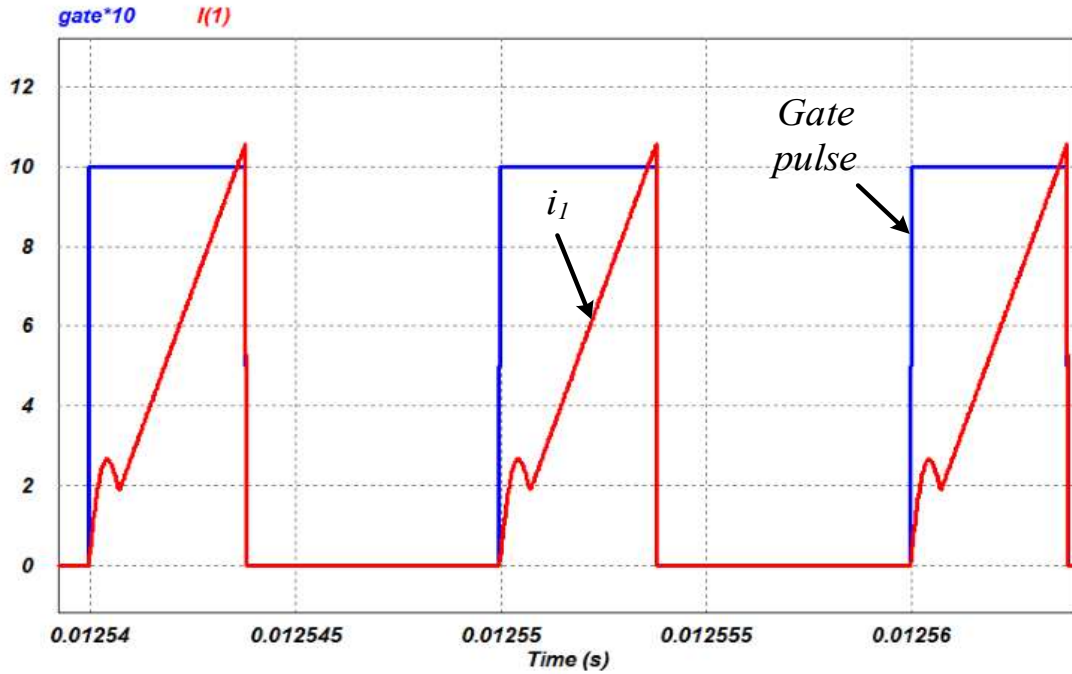
Figure 2-7 Primary switch current (i_1) and gate pulses.
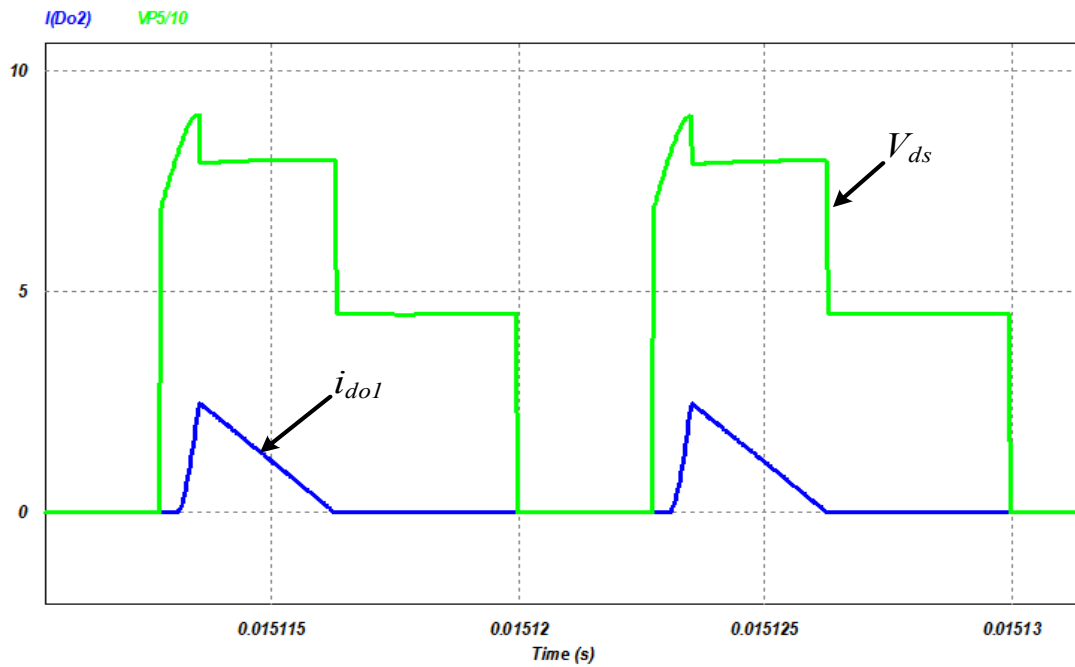
Figure 2-8 Voltage across switch S$_1$ (v_{ds}) and secondary diode current (i_{do2}).
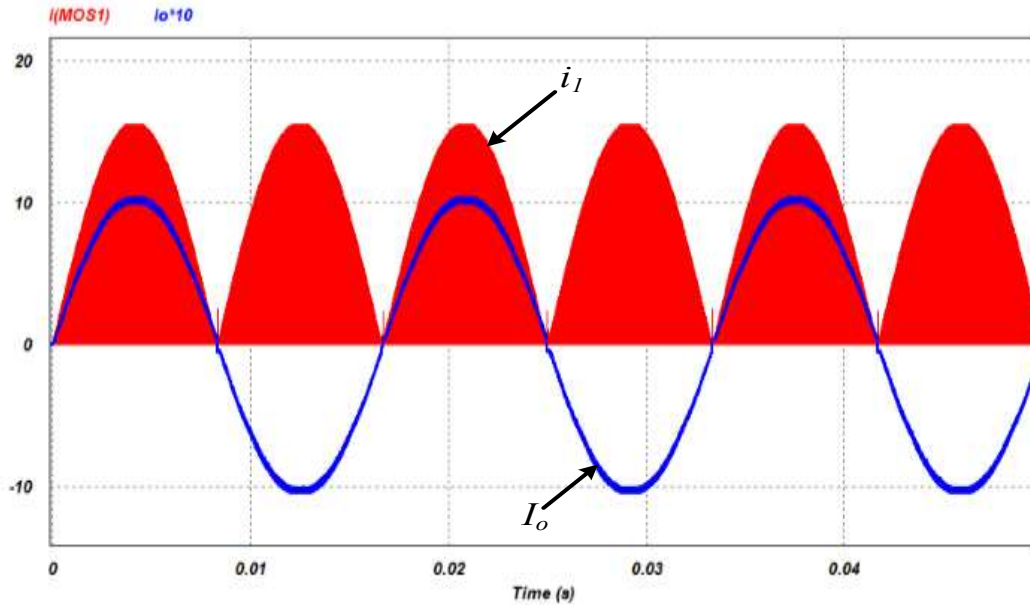
Figure 2-9 primary switch current (i_1) and load current (I_o) .

2.5   Experimental Results

An experimental prototype of the flyback microinverter was built to confirm its feasibility. An *110VAC* inverter was built according to the following specifications: input voltage V_{in} = *45VDC*, maximum output power $P_{o,max}$ = *100W* and switching frequency f_s=*100 kHz*. A TMS320f28335 DSP was used to generate the gating signals for the primary and the secondary switches.

The main switch current and the current through diode D_2 of the snubber are shown in Figure 2-10. It can be seen that current flows through D_2 for only a small portion of the switching cycle. The voltage across and the current through primary switch S_1 are shown in Figure 2-11. In Figure 2-12, the primary current, secondary current, and the voltage across the clamp capacitor are shown. In Figure 2-13, the switch current, output current, and the snubber current throughout the AC cycle are shown.

46
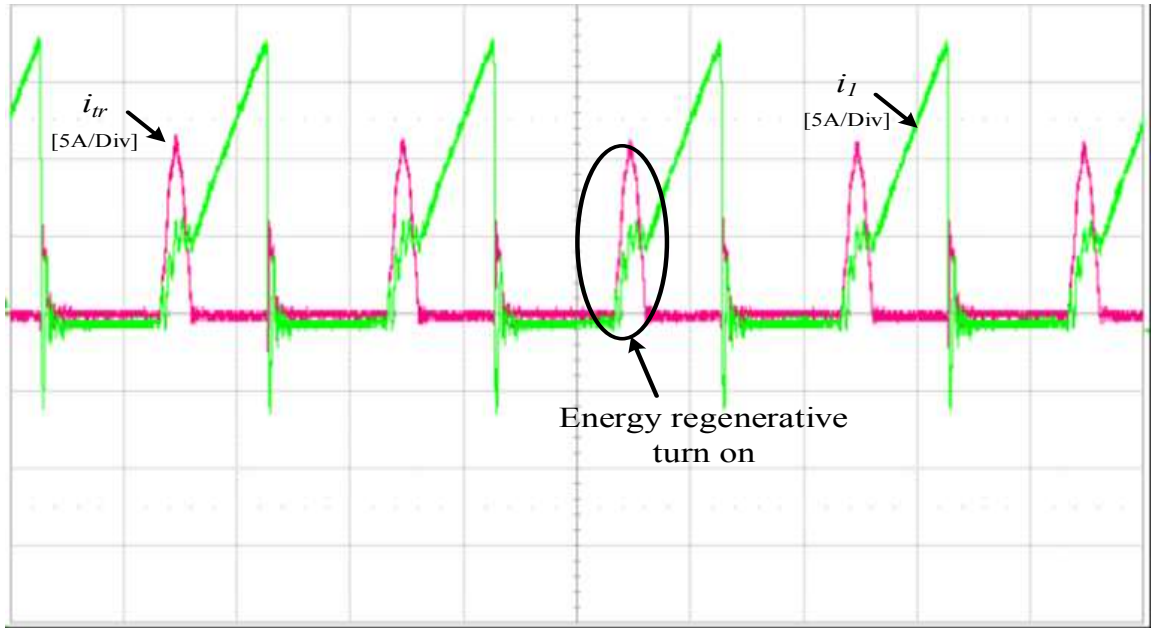
Figure 2-10 Regenerative current (i_{tr}) and primary switch current (i_1).
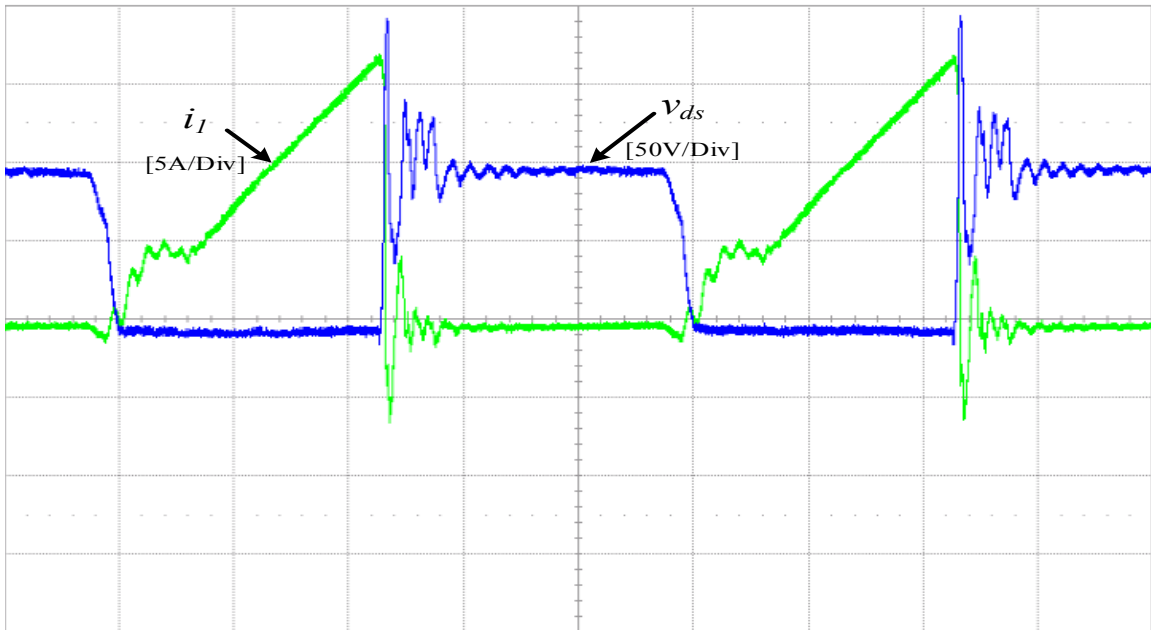
Figure 2-11 Primary switch current (i_1) and voltage across S$_1$ (v_{ds}).
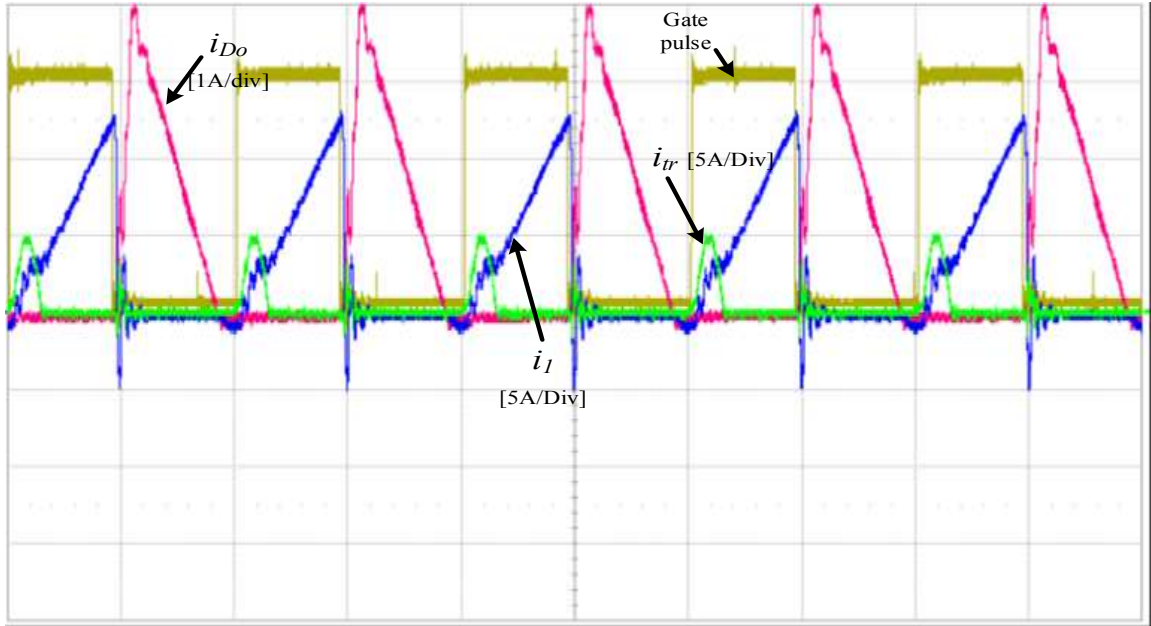
Figure 2-12 Regenerative current (i_{tr}), primary switch current (i_1) and secondary diode current (i_{do1}).
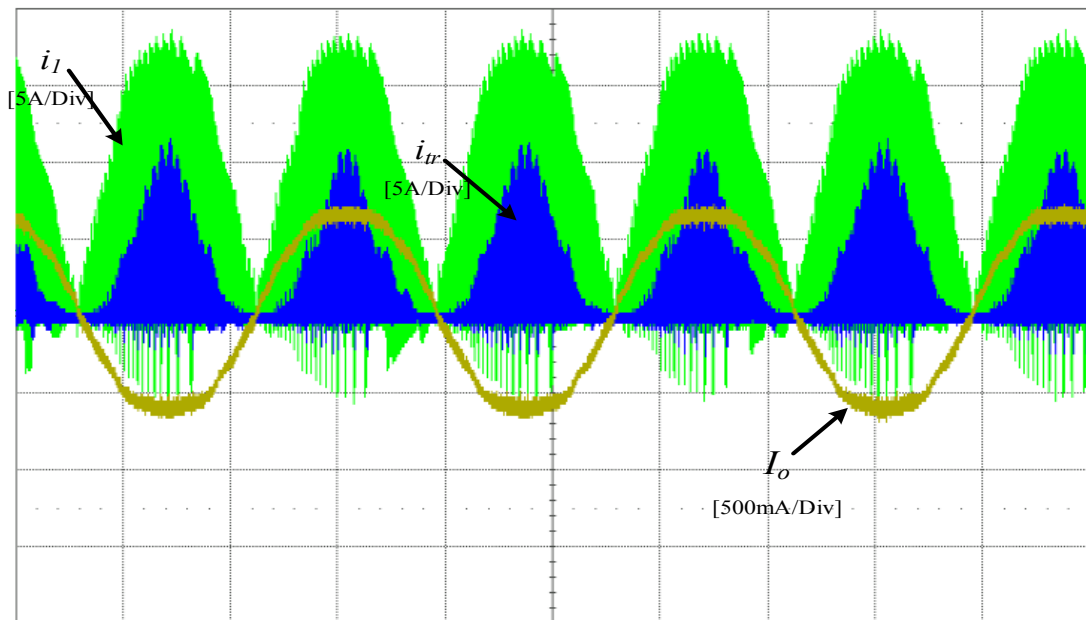
Figure 2-13 Regenerative current (i_{tr}), primary switch current (i_1) and load current (I_o).

A graph of converter efficiency vs. load comparison for the cases when the converter is implemented with the passive snubber and with a resistor-capacitor-diode (RCD) snubber is shown in Figure 2-14. It can be seen that a maximum gain in efficiency of 5%-6% can be achieved by using the passive snubber instead of the RCD snubber.
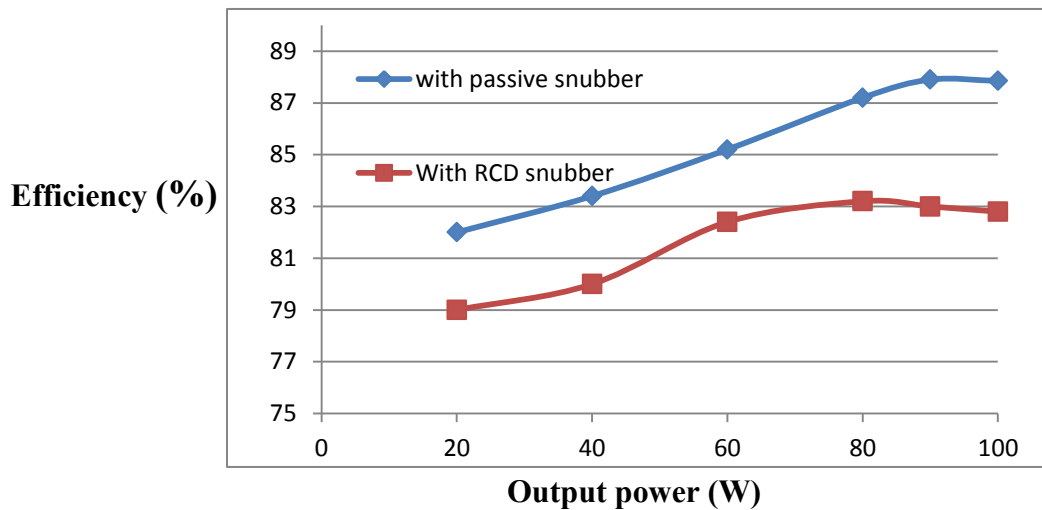
Figure 2-14 Efficiency comparison

2.6   Conclusion

A low cost technique for improving the efficiency of a basic DC-AC flyback micro-inverter is proposed in the paper. The proposed efficiency improving technique is based on a simple snubber, consisting of just a few passive elements. In the paper, the flyback microinverter with the passive snubber is presented and the reasons as to why a passive snubber is being proposed are stated. The modes of operation of the converter are discussed and analyzed and the design of the converter is reviewed.

Experimental results obtained from a lab prototype have been presented in this proposal and show that a 5% improvement in efficiency over the use of conventional RCD snubbers can be achieved simply by replacing the resistor R with a diode and implementing an auxiliary winding in the main power transformer. This is a significant efficiency gain that can be achieved without the use of more sophisticated ZVS and ZCS active snubber techniques, taking advantage of the typical specifications of microinverters in solar energy systems.

Chapter 3

3 Proposed Quasi-Resonant Flyback Micro-Inverter with Energy Regenerative Snubber

It was found in the previous chapter that adding a simple regenerative snubber to a flyback micro-inverter can improve its efficiency significantly. Although the snubber circuit can reduce the turn-off losses of the primary switch, the converter's efficiency can be further improved if the turn-on losses of the primary switch are reduced as well. Since MOSFETs are switching devices that are typically used in micro-inverters, doing so involves the use of zero-voltage switching (ZVS) techniques [43-50].

A new flyback micro-inverter that combines the use of a ZVS technique and an energy regenerative snubber is proposed in this chapter. As this ZVS technique is based on quasi-resonant circuit principles, these principles are briefly reviewed and the operation of the new micro-inverter is explained in detail. The design of the converter is discussed and demonstrated with an example. The feasibility of the new converter is confirmed with simulation and experimental results.

3.1 Basic Quasi-resonant DC-DC Flyback Converter

The basic principle behind the ZVS operation of a converter that uses a MOSFET device as its main switch is that current must flow through its internal body-diode before it is turned on. Doing so ensures that there is no energy stored in its output capacitance (which can be a combination of the device's internal output capacitance and additional external capacitance) when the switch is turned on so that this energy is not dissipated in the

switch. The power loss that is associated with the switch output capacitance can be expressed as

$$P_{loss\_on} = \frac{1}{2} C_s v_{ds}^2 f_s \tag{3.1}$$

Where f_s is switching frequency and v_{ds} is voltage across the drain and source of the MOSFET.

A simple way to implement a converter with ZVS is to use quasi-resonant circuit [44-50] principles as this may involve the addition of a few passive elements and the use of additional active auxiliary switches is avoided. In the case of the quasi-resonant DC-DC flyback converter that is shown in Figure 3-1, the converter topology is identical to that of a standard flyback converter as it already has the passive elements needed to ensure quasi-resonant operation. Typical converter waveforms for the case when the converter is operating with its magnetizing inductance L_m in discontinuous current mode (DCM) are shown in Figure 3-2.
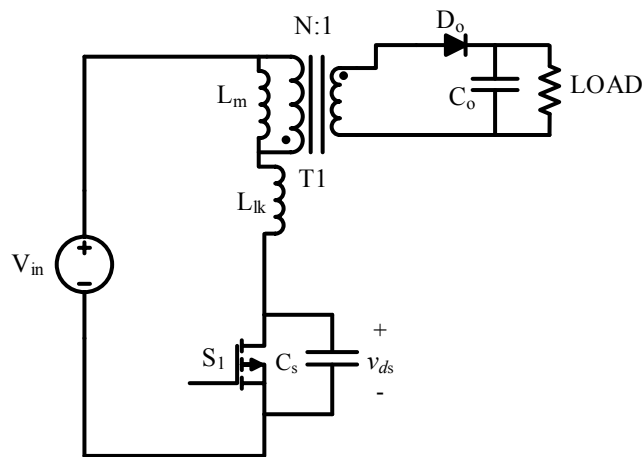
Figure 3-1 DC-DC quasi-resonant converter.
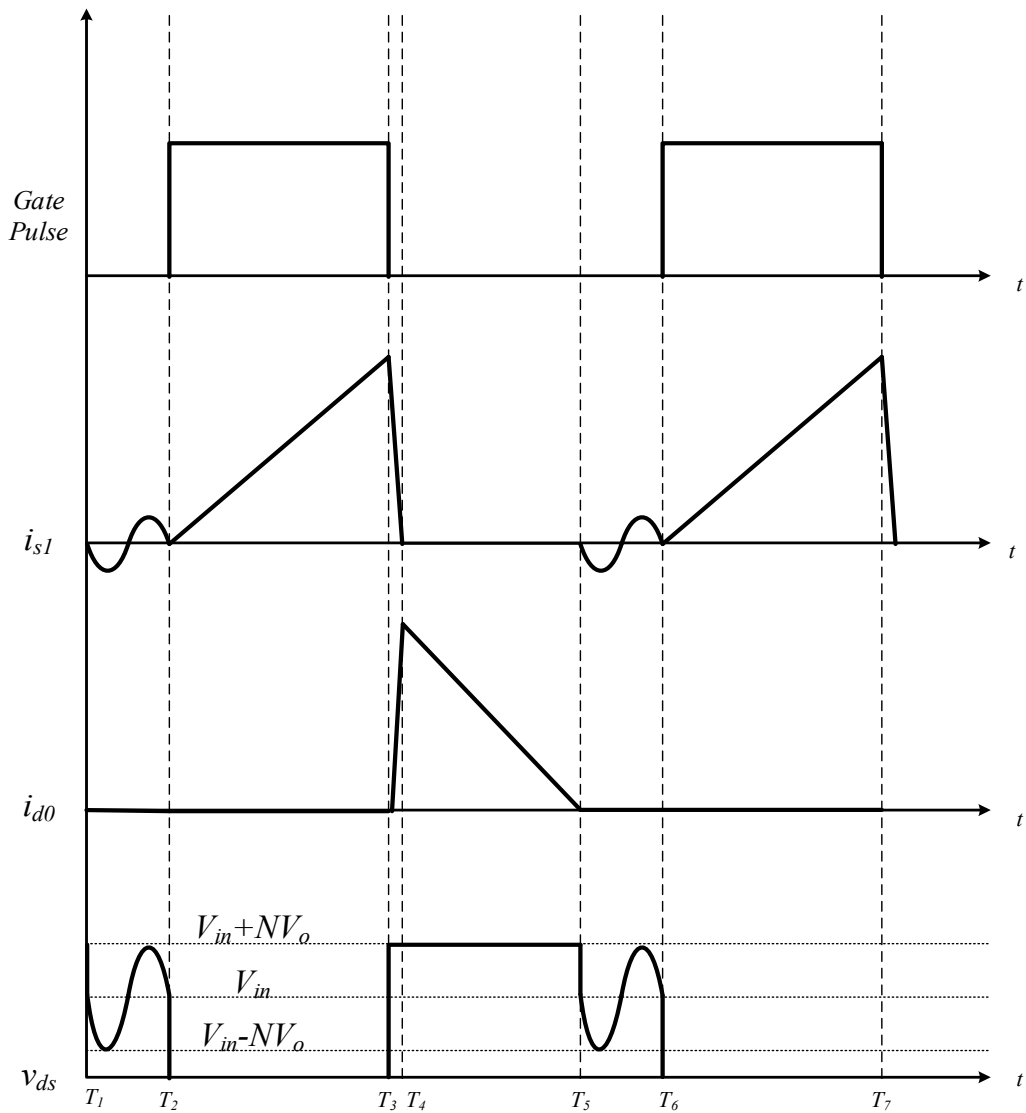
Figure 3-2 Typical operating waveform of a DCM flyback converter.

Since the converter is operated with L_m in DCM, the secondary current ceases conduction before the primary switch is turned on. It can be seen in Figure 3-2 that the primary current (i_{s1}) starts resonating as the secondary diode D_0 ceases conduction at $t=T_1$ and T_5. This resonance is caused by the interaction of the output capacitance of the switch and magnetizing inductance L_m. As the secondary current become zero, the primary and

secondary windings become decoupled so that the voltage across the primary winding is no longer NV_0 and thus the switch output capacitance C_s can resonate with L_m. This C_s to discharge and then recharge back as the voltage across the switch (v_{ds}) swings between V_{in}-NV_0 to V_{in}+NV_0. According to equation (3.1), the maximum switching loss is at the peak voltage (V_{in}+NV_0) and the minimum at the valley (V_{in}-NV_0). If the converter is always switched at the voltage valley (V_{in}-NV_0), then switching losses can be reduced and converter efficiency can be improved.

What is key is knowing when the voltage valley occurs so that the switch can be turned on at the right time. This time is dependent on the time period of the resonant cycle caused by the interaction of L_m and C_s, T_r. This resonant cycle occurs just after the transformer can be completely demagnetized and the transformer secondary current falls to zero, during the interval T_1-T_2 and T_5-T_6 in Fig. 3-2. From the equivalent circuit for this interval shown in Figure 3-3, the period of the resonant cycle (T_r) can be determined to be

$$T_r = 2\pi\sqrt{(L_m + L_{lk})C_s} \qquad (3.2)$$

It can be seen from Figure 3-2 that the voltage across the switch (v_{ds}) reaches its minimum value at the half of the resonant cycle ($T_r/2$) and that the switch capacitance begins to be recharged afterwards. If the converter switch is turned on at time

$$\frac{T_r}{2} = \pi\sqrt{(L_m + L_{lk})C_s} \qquad (3-3)$$

after the secondary current reaches zero, this will ensure minimum turn-on switching loss. This means that the converter must be operated with variable switching frequency
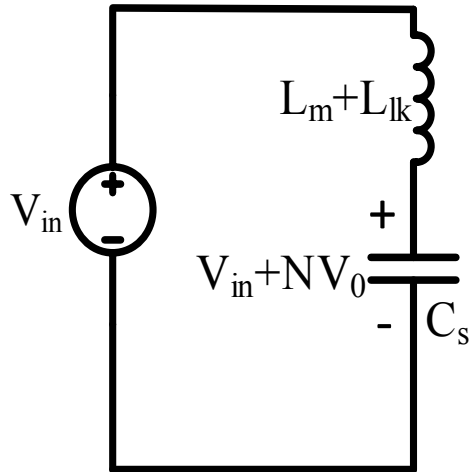
Figure 3-3 Equivalent circuit for period (T_1-T_2) and (T_5-T_6).

throughout the line and load rage as the switch must be turned on at time $T_r/2$ after the secondary current falls to zero and this event varies throughout the line and load range.

In order to ensure that the switch can turned on with ZVS, that is for the switch voltage valley to reach zero, the converter should be designed so that the reflected voltage should be at least equal with the input voltage, according to

$$V_{in} \leq NV_0 \tag{3.4}$$

If this can be done, then the switch voltage waveform looks like what is shown in Figure. 3-4.
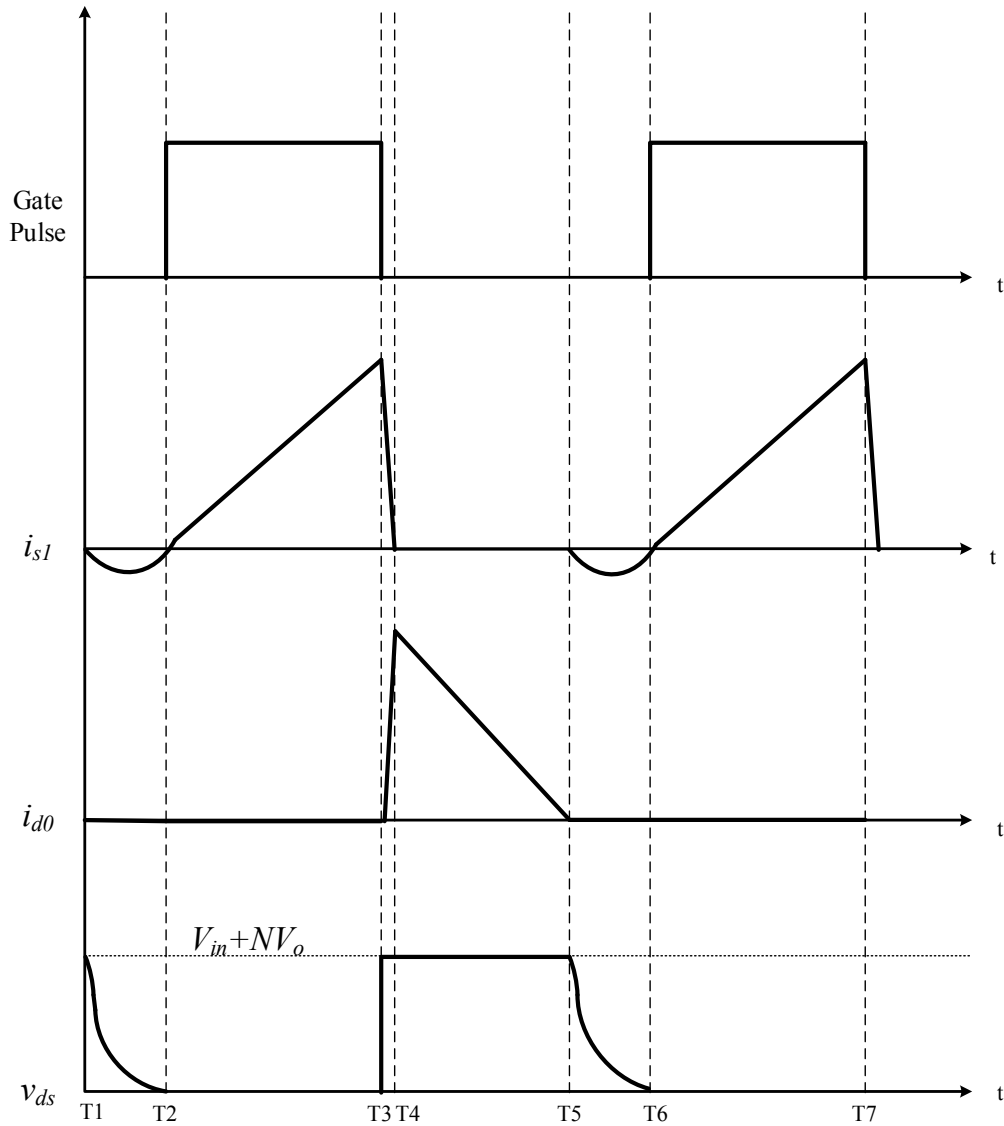
Figure 3-4 Typical operating waveform of a variable frequency DCM.

3.2 Proposed regenerative snubber based quasi-resonant flyback inverter

Using the quasi-resonant principles discussed in the previous section, a new flyback micro-inverter can be proposed. This micro-inverter has the same topology as the one presented in the previous chapter, but it is operated as a quasi-resonant converter with

variable switching frequency. In this section, the converter's modes of operation are discussed and the converter is analyzed so that the necessary conditions for ZVS operation can be determined. An example showing how the converter can be designed is presented along with simulation results and experimental results obtained from a lab prototype.

3.2.1   Converter operation

Since the operation of the converter is very similar to the one presented in the previous chapter, the modes of operation are only briefly reviewed here. Figure 3-6 shows the key operating modes and typical operating waveforms are given in Figure 3-7.

Mode 1

This mode begins when the primary switch S_1 is turned on at $t=T_0$. As the switch is turned on, the input voltage is impressed across the transformer primary and starts charging the magnetizing inductance (L_m). This mode ends as the auxiliary diode D_2 becomes reverse biased and stop conducting at $t=T_1$.

Mode 2 -4

Modes 2, 3 and 4 are similar with the modes of the converter presented in the previous chapter. Energy continues to be stored in the transformer during Mode 2 and in Mode 3, after the primary switch is turned off; the energy stored in the leakage inductance of the transformer is transferred to the clamp capacitor during Mode 3. In Mode 4, a secondary diode conducts and the stored energy in the magnetizing inductance of the transformer is transferred to the load.

Mode 5

This mode begins when the secondary current falls to zero. When this happens, the transformer primary and secondary windings become decoupled so that the primary voltage is no longer equal to the reflected output voltage, NV_o; this allows diode D_2 to become forward biased if the voltage across the clamp capacitor (v_{clamp}) is high enough. The conduction of D_2 is dependent on the resonant interaction between the equivalent inductance and the clamp capacitance, C_{clamp}. The duration of this resonant cycle is half the resonant period as diode D_2 then becomes reverse biased. ZVS can be achieved at the end of this resonant period, at time T_5, if the sum of the auxiliary winding voltage and the clamp capacitor voltage is zero.

The time period of this resonant cycle (T_{qr}) can be determined from the resonant circuit shown in the Figure 3-5,
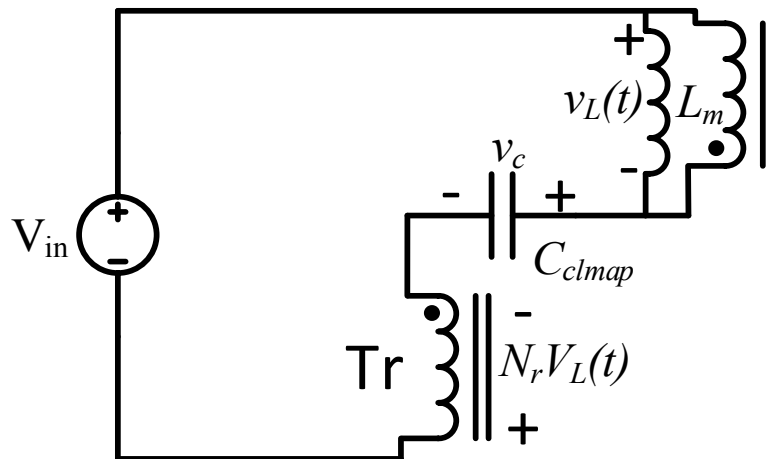
Figure 3-5 Resonant circuit for mode 5.

From this circuit the equation can be written as,

$$V_{in} = L_m \frac{di_1}{dt} + \frac{1}{C} \int i_1 \, dt - N_r L_m \frac{di_1}{dt} \tag{3.5}$$

By differentiating both side equation (3.5) can be written as,

$$0 = L_m \frac{d^2 i_1}{dt^2} + \frac{1}{C} i_1 - N_r L_m \frac{d^2 i_1}{dt^2} \tag{3.6}$$

Equation (3.6) can be simplified as

$$(N_r - 1) L_m \frac{d^2 i_1}{dt^2} = \frac{1}{C} i_1 \tag{3.7)}$$

By further rearrangement it can be written as,

$$C_{clamp}(1 - N_r) L_m \frac{d^2 i_1}{dt^2} + i_1 = 0 \tag{3.8)}$$

Transferring equation (3.8) to Laplace domain,

$$C_{clamp}(1 - N_r) L_m s^2 + 1 = 0 \tag{3.9}$$

Therefore, equation (3.9) can be written as,

$$s = J \frac{1}{\sqrt{C_{clamp}(1 - N_r) L_m}} \tag{3.10}$$

From equation (3.10) the resonant frequency (ω_{qr}) can be written as,

$$\omega_{qr} = \frac{1}{\sqrt{C_{clamp}(1 - N_r) L_m}} \tag{3.11}$$

Therefore this resonant time period is given by,

$$T_{qr} = 2\pi\sqrt{C_{clamp}(1 - N_r)L_m} \qquad (3.12)$$

From equation (3.11) total time period of a switching cycle including half of the resonant period can be written as,

$$T_s(t) = T_{on}(t) + T_{do}(t) + T_{qr}/2 \qquad (3.13)$$

Where T_{on} is the required on-time to ensure a ZVS turn-on and T_{do} is the secondary diode conduction time. The converter duty cycle d_1 can also be defined as the ratio T_{on}/T_s.

It should be noted that the duty cycle is varied in a sinusoidal manner to produce a sinusoidal output. This means that the clamp capacitor stores more charge when the duty cycle is at its peak value and less charge when the duty cycle is at its minimum. As a result, for very low duty cycles, the voltage across the capacitor is such that diode D_2 remains reverse biased and Mode 5 may not occur.
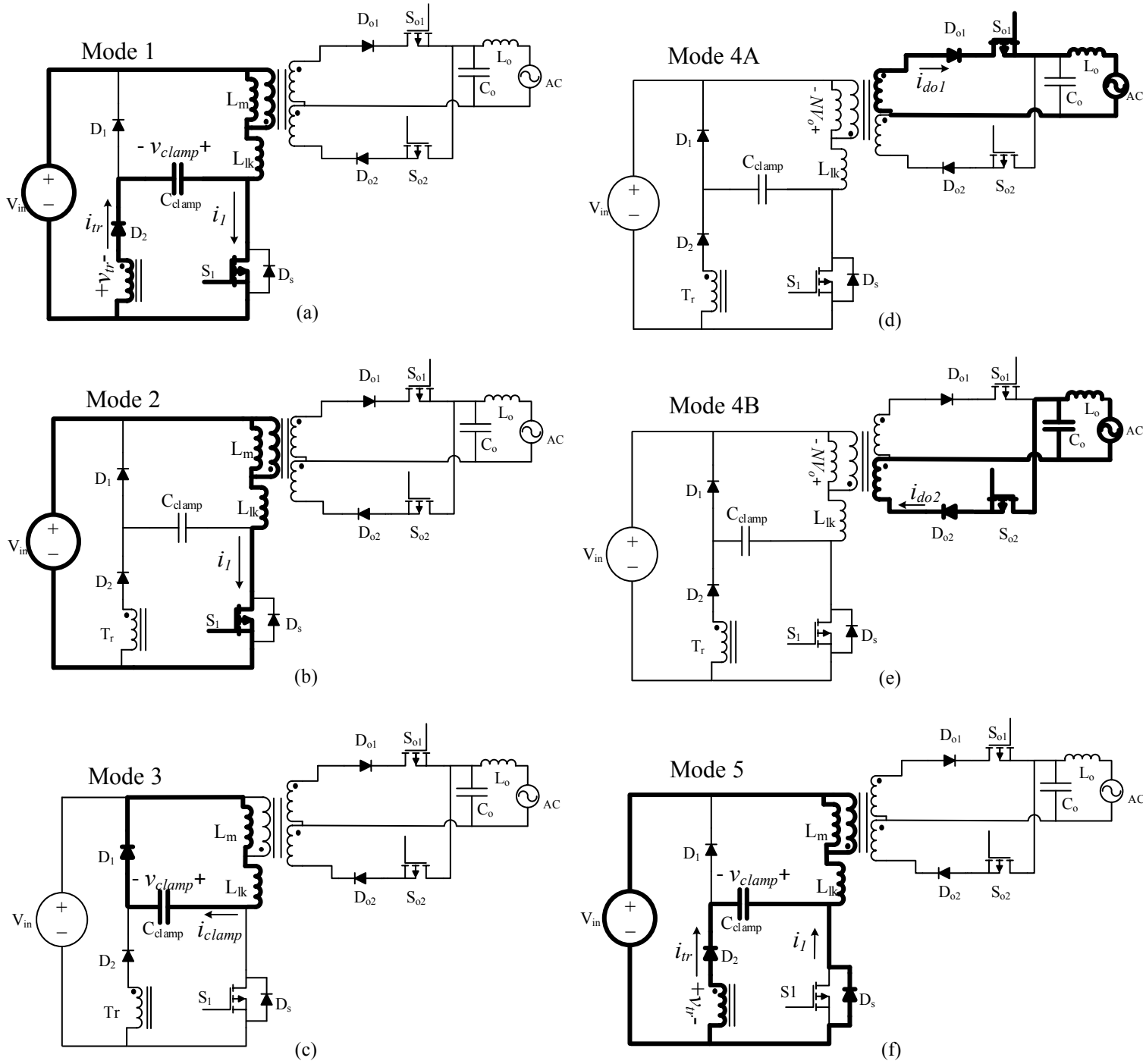
Figure 3-6 Operating modes (Note: Mode 4 is divided into (d) and (e) depending on the polarity of the 60 Hz AC sine wave).
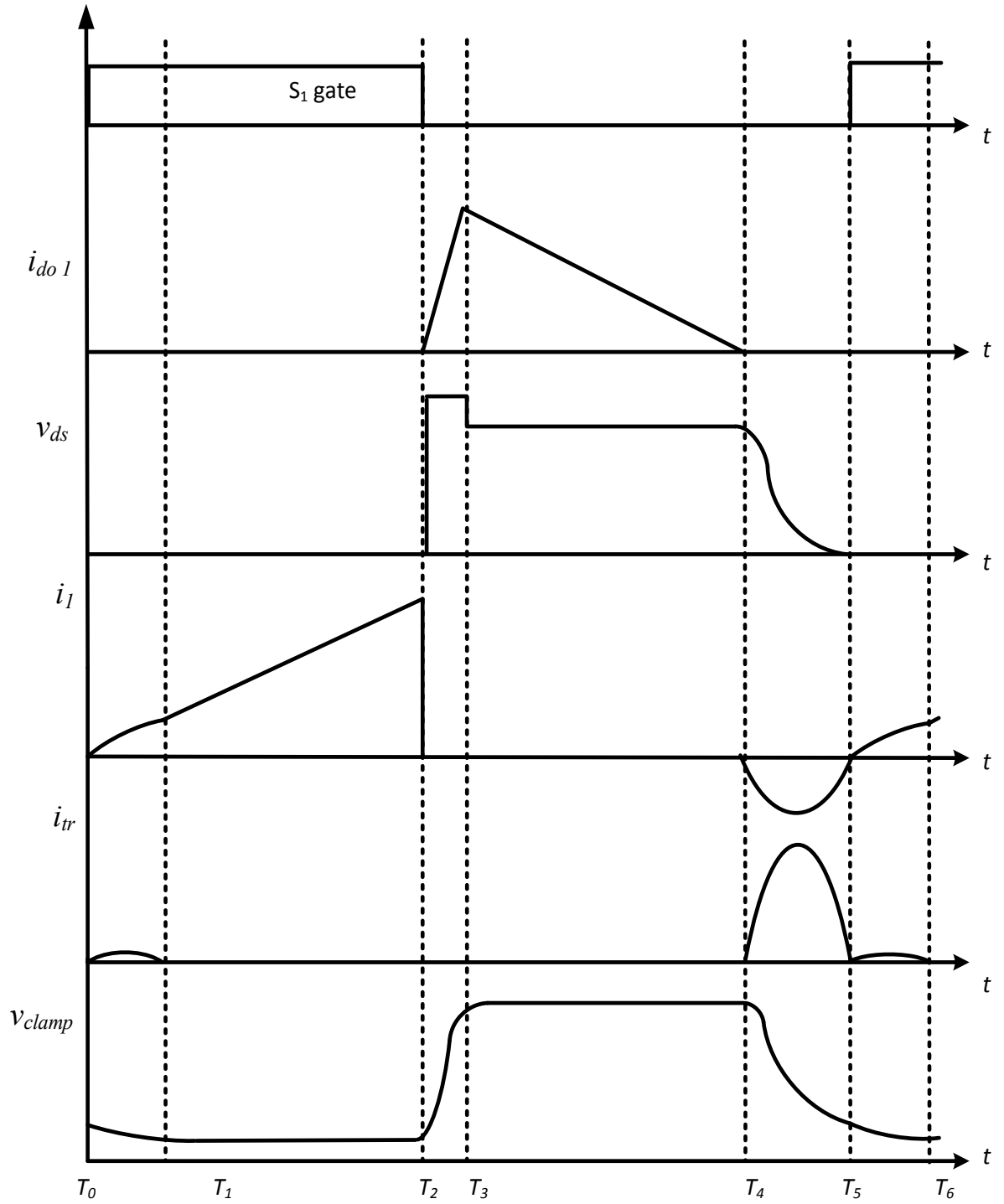
Figure 3-7 Typical converter waveforms.

3.2.2 Zero voltage turn on (ZVS) conditions

If the sum of the clamp capacitor voltage and auxiliary winding becomes zero during Mode 5 (Figure. 3-6(f)), then the voltage across switch S_1 is forced to be zero and the switch can turn on with ZVS. This is possible if diode D_2 can conduct during this mode. To ensure that this happens, the voltage across the switch (v_{ds}) before the start of the resonant cycle (after the secondary current falls to zero) needs to be determined to confirm that it is possible for diode D_2 to be forward biased during Mode 5.

Figure 3-9 gives the equivalent voltage sources in the circuit while a secondary diode conducts (Mode 4 – Figure. 3-6(d) or (e)). From Figure 3-9, it can be seen that there is a reflected voltage NV_o across the primary winding as a secondary diode conducts and a voltage N_rNV_o appears across the auxiliary winding as well. During this time, the clamp capacitor voltage is at its maximum value. The voltage (v_{ds}) across the primary switch before the start of the resonant cycle at Mode 5 is

$$v_{ds}(t) = V_{in} + NV_0(t) \tag{3.14}$$
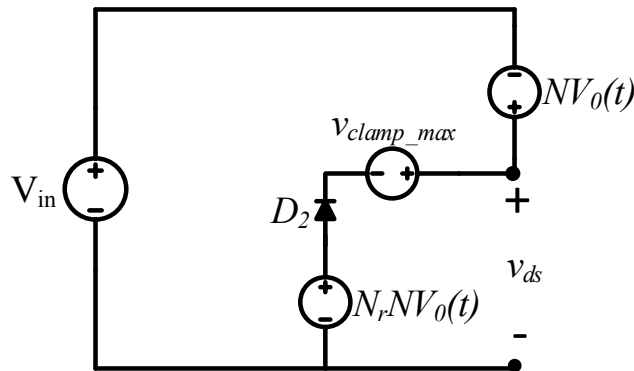
Figure 3-8 Voltage sources during T_3-T_4.

A detailed waveform of the voltage (v_{ds}) across the switch is given in Figure 3-10. For normal flyback operation, the reflected voltage at the primary becomes zero when the secondary current falls to zero at $t=T_4$. For this converter, however, as the reflected voltage drops by $v_x(t)$, the sum of reflected voltage at the primary (NV_0- $v_x(t)$) and the input voltage (V_{in}) becomes equal to the sum of the clamp capacitor voltage (v_{clamp_max}) and the reflected voltage at the auxiliary winding (N_rNV_0). As a result, the voltage across diode D_2 becomes zero and current can flow through the auxiliary winding. Using the initial value of v_{ds} from equation (3.6) and the equivalent circuit in Figure 3-8, the following equation based on Kirchoff's Voltage Law can be written:

$$V_{in} + NV_o(t) - v_x(t) = v_{clmap\_max}(t) + N_r v_r(t) \qquad (3.15)$$

It can be seen from Figure 3-9 that the reflected voltage becomes $v_r(t)$ when the reflected voltage to the primary drops by voltage $v_x(t)$ so that equation (3.10) can be written in terms of reflected instantaneous voltage $v_r(t)$ as

$$V_{in} + NV_o(t) - \left(NV_o(t) - v_r(t)\right) = v_{clmap\_max}(t) + N_r v_r(t) \qquad (3.16)$$

which can be simplified to be

$$V_{in} + v_r(t) = v_{clmap\_max}(t) + N_r v_r(t) \qquad (3.17)$$

Rearranging this equation gives

$$v_r(t) = \frac{v_{clmap\_max}(t) - V_{in}}{1 - N_r} \qquad (3.18)$$

Which is the reflected voltage at the point from where D_2 turns on and the resonant cycle starts. The determination of this voltage is important because this voltage level sets the range in the AC cycle where the converter can operate with ZVS, as will be explained later in this chapter.
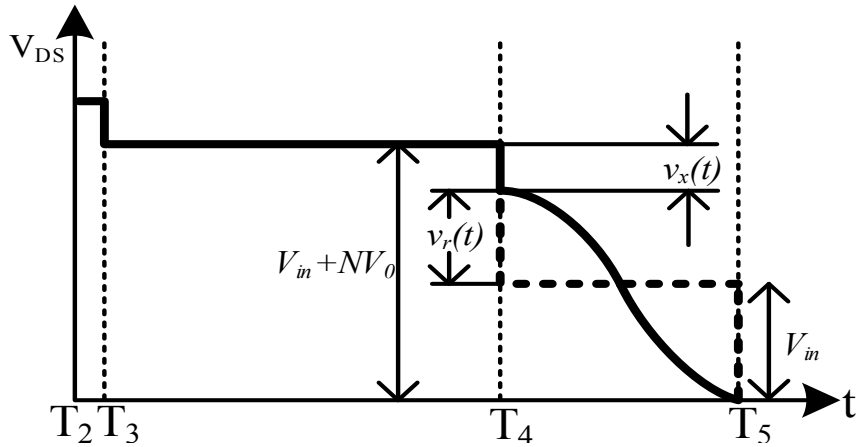
Figure 3-9 Voltage across switch S_1 during ZVS.

Since the sum of the clamp capacitor voltage and auxiliary winding voltage need to be zero at the end of the resonant mode (Mode 5 at T_5), these voltages need to be determined. To find the voltage across the capacitor C_{clamp} at T_5, its initial condition at the start of the resonant mode (at T_4) need to be determined. From equation (3.12), the clamp capacitor voltage (v_{clamp_max}) at the start of the resonant cycle is

$$v_{clmap\_max}(t) = V_{in} + v_r(t) - N_r v_r(t) \tag{3.19}$$

If the change in reflected voltage during Mode 5 is taken as Δv_r, then the change in capacitor voltage (Δv_{clamp}) during this resonant mode can be derived from equitation

65

(3.14). As input voltage is fixed, the change in capacitor voltage (Δv_{clamp}) can be expressed as

$$\Delta v_{clmap}(t) = \Delta v_r(t) - N_r \Delta v_r(t) \tag{3.20}$$

It can be seen from Figure 3-9 that the reflected voltage starts resonating from $+ v_r(t)$ so that $v_r(t)$ swings from $+ v_r(t)$ to $- v_r(t)$ and the change in reflected voltage can be expressed as

$$\Delta v_r(t) = 2 * v_r(t) \tag{3.21}$$

Substituting this equation into equation (3.15) gives

$$\Delta v_{clmap}(t) = 2(v_r(t) - N_r v_r(t)) \tag{3.22}$$

For ZVS operation, the sum of the capacitor voltage and reflected auxiliary winding voltage should be zero at the end of the resonant cycle (end of Mode 5). The relation between the clamp capacitor voltage and auxiliary winding voltage at the end of Mode 5 can be written as

$$[v_{clmap\_max}(t) - \Delta v_{clmap}(t)] - [N_r v_r(t) - N_r \Delta v_r(t)] = 0 \tag{3.23}$$

As $v_r(t)$ swings from $+ v_r(t)$ to $- v_r(t)$, the reflected voltage at the auxiliary winding at T_5 becomes $-N_r v_r(t)$; therefore the condition for ZVS turn-on in equation (3.16) can be simplified to be

$$v_{clmap\_max}(t) - \Delta v_{clmap}(t) - N_r v_r(t) = 0 \tag{3.24}$$

66

With the above conditions satisfied, the primary switch needs to be turned on after a time of half of the resonant period ($T_{qr}/2$), after the secondary current falls to zero. To achieve this, the converter must be made to operate with variable switching frequency. If the converter's switching frequency is varied to accommodate exactly half of the resonant period ($T_{qr}/2$) for different duty cycles, a ZVS turn-on of the primary switch can be achieved over a wide range of the AC cycle.

Since the converter's switching frequency is variable, then so too is the length of its switching cycle. From equation (3.5) and Figure 3-10, the period of the switching cycle can be expressed as

$$T_s(t) = T_{on}(t) + T_{do}(t) + \frac{T_{qr}}{2} \tag{3.25}$$

and the length of time that a secondary diode conducts (Mode 4) can be expressed as

$$T_{do}(t) = T_s(t) - \left[d_1(t)T_s(t) + \frac{T_{qr}}{2} \right] \tag{3.26}$$

where $d_1(t)$ and $T_s(t)$ are required duty cycle and time period for any particular cycle.
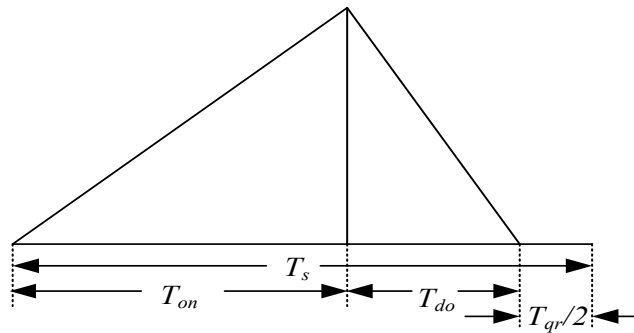
Figure 3-10 Switching time.

The duration of Mode 4 depends on the current that is flowing in the circuit and is longest when the maximum peak current is flowing. From equation 2.13, peak primary current i_{1_pk} for any particular cycle can be written as

$$i_{1\_pk}(t) = \frac{V_{in}d_{1\_pk}(t)T_S(t)}{L_m} \tag{3.27}$$

Which can be rearranged to give

$$T_{on}(t) = \frac{i_{1\_pk}(t)L_m}{V_{in}} \tag{3.28}$$

As $T_{on} = d_{1\_pk}T_s$. Similarly from equation (2.9), the following expressed can be written

$$i_{1pk}(t) = \frac{NV_0(t)[1-d_1(t)]T_S(t)}{L_m} \tag{3.29}$$

Which can be rearranged to give the following expression for secondary diode conduction time:

$$T_{do}(t) = \frac{i_{1\_pk}(t)L_m}{NV_0(t)} \tag{3.30}$$

From equations (3.4), (3.18) and (3.20), the resonant period, switch turn-on time and turn off-time can be determined so that the total time period for any particular switching interval can be given by

$$T_s(t) = T_{on}(t) + T_{do}(t) + \frac{T_{qr}}{2} = T_s(t) = \frac{i_{1\_pk}(t)L_m}{V_{in}} + \frac{i_{1\_pk}(t)L_m}{NV_0(t)} + \frac{T_{qr}}{2} \tag{3.31}$$

which can be rewritten as

$$T_s(t) = i_{1\_pk}(t)L_m\left[\frac{1}{V_{in}} + \frac{1}{NV_0(t)}\right] + \frac{T_{qr}}{2} \tag{3.32}$$

Since

$$f_s(t) = \frac{1}{T_s(t)} = \text{Switching frequency} \tag{3.33}$$

Equation (3-28) can be rewritten as

$$f_s(t) = \left[i_{1\_pk}(t)L_m \left(\frac{1}{V_{in}} + \frac{1}{NV_0(t)} \right) + \frac{T_{qr}}{2} \right]^{-1} \tag{3.34}$$

So that a relationship between switching frequency, duty cycle and circuit parameters can be established.

3.3 Design Considerations

In this section, the design of the proposed flyback inverter is described. The main consideration that must be taken into account is that the primary switch is turned on with ZVS with the converter operating with variable switching frequency. The converter is designed according to the following specifications: Input voltage 40-50V, Output voltage 110V, and maximum output power 100W.

The procedure is iterative and only the final iteration is shown here. It is very similar to that of the converter presented in the previous chapter so that based on previous iterations, it was determined that the magnetizing inductance L_m = 12.8 µH in the previous chapter is satisfactory for this particular converter because its power levels are same.

3.3.1 Turns ratio selection

The ZVS conditions mentioned in section 3.3.2 it was determined that if the reflected voltage is higher, reflected voltage to auxiliary winding will also be higher and increasing the reflected voltage will help in achieving ZVS for a wider range. Therefore to design

the converter such that ZVS can be achieved, turns ratio need to be selected at first, so that the amount of reflected voltage can be estimated.

From equation (3.24) it is derived that, for ZVS turn on reflected voltage at the auxiliary winding should be greater or equal with the capacitor voltage at the end of resonant cycle. Therefore, variation in capacitor voltage (v_{clamp}) and auxiliary winding voltage at the end of the resonant mode throughout the AC cycle need to be determined, which is given in Figure 3-11. It can be seen from this graph that, by increasing turns ratio from 0.33 to 0.4 the ZVS range can be increased and by further increasing the turns ration will impose a higher reflected voltage but it will also create high voltage stress across the MOSFET. Also for higher turns ratio duty cycle need to be increased, this will push the converter toward continuous conduction mode. Therefore considering all these parameters turns ratio ($N_p/N_s=N$) is chosen as 0.4.
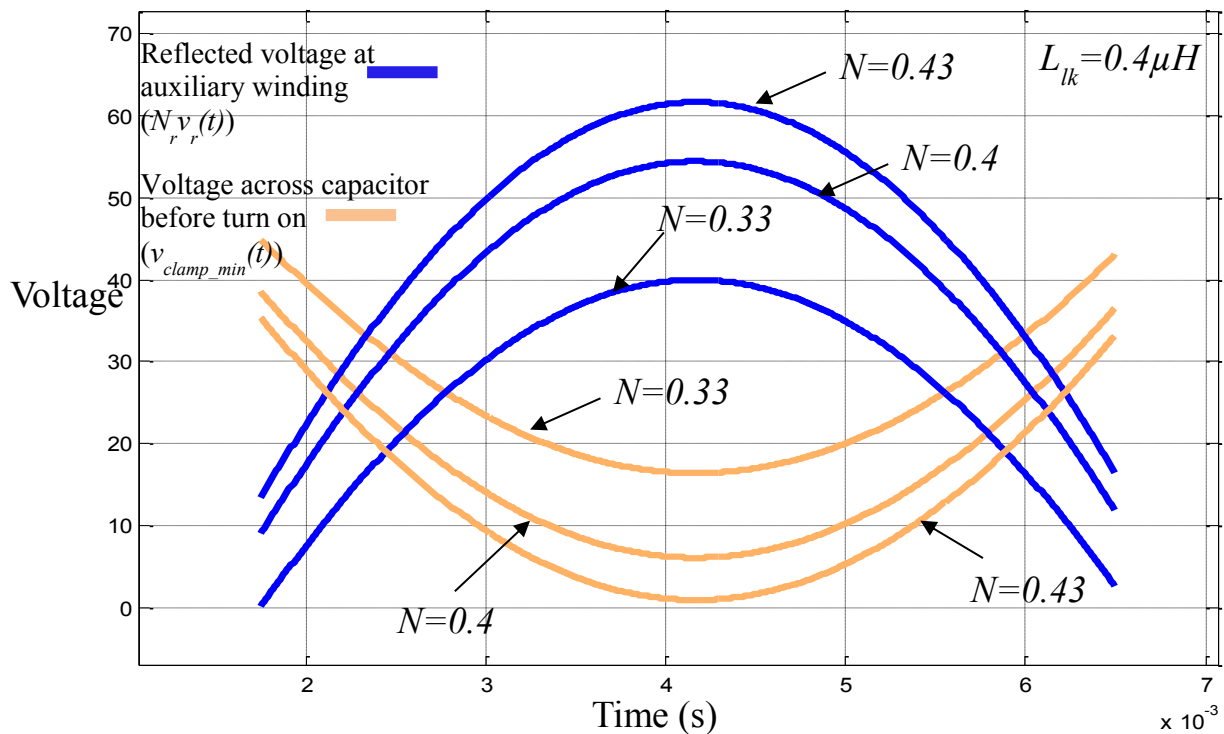

Figure 3-11 Variation in capacitor and auxiliary winding voltage for half AC cycle.

3.3.2 Maximum Duty cycle

Maximum duty cycle and turns ratio is interrelated for a fixed voltage gain, if the converter is operated in DCM. The relation between them was derived in equation (2.12). The turn's ratio for this converter is increased to 0.4 to achieve a better ZVS range. As the converter is operated in DCM the value of the peak duty cycle can be determined from equation (2.12), the peak duty cycle is given by,

$$d_{pk} = \frac{1}{\frac{V_{in}}{NV_{grid\_pk}}+1} = \frac{1}{\frac{50}{0.4*155}+1} = 0.6 \tag{35}$$

3.3.3   Clamp capacitor selection

The clamp capacitor value is critical to ensure ZVS operation. In Section 3.2.2, it was stated that the clamp capacitor voltage should be such that the sum of the voltage across it (v_{clamp}) and the auxiliary winding is greater than the sum of input voltage and the reflected voltage at the primary winding. Otherwise diode D_2 remains reverse biased and the resonant mode needed for the ZVS turn-on of the primary switch cannot begin. What this means is that the clamp capacitor should be small enough so that sufficient voltage should appear across it. It should not be too small, however, as the voltage across it should not be too high or else a considerable voltage spike will appear across the switch.

The voltage rise across clamp capacitor can be determined from equation (2.43) and this voltage rise is plotted in Figure 3-12 for different values of peak current. It can be seen from this graph if the capacitor value is decresed voltage across it will increse. Therefore to increse the voltage across the capacitor so that the resonant cycle can start and considering the trade off of higher voltage stress across the MOSFET, capacitor value is reduced to 0.12 μF.

Voltage rise acr... ...apacitor (δv_{clamp})

$i_{1\_pk}=20A$

$i_{1\_pk}=15A$

$i_{1\_pk}=10A$
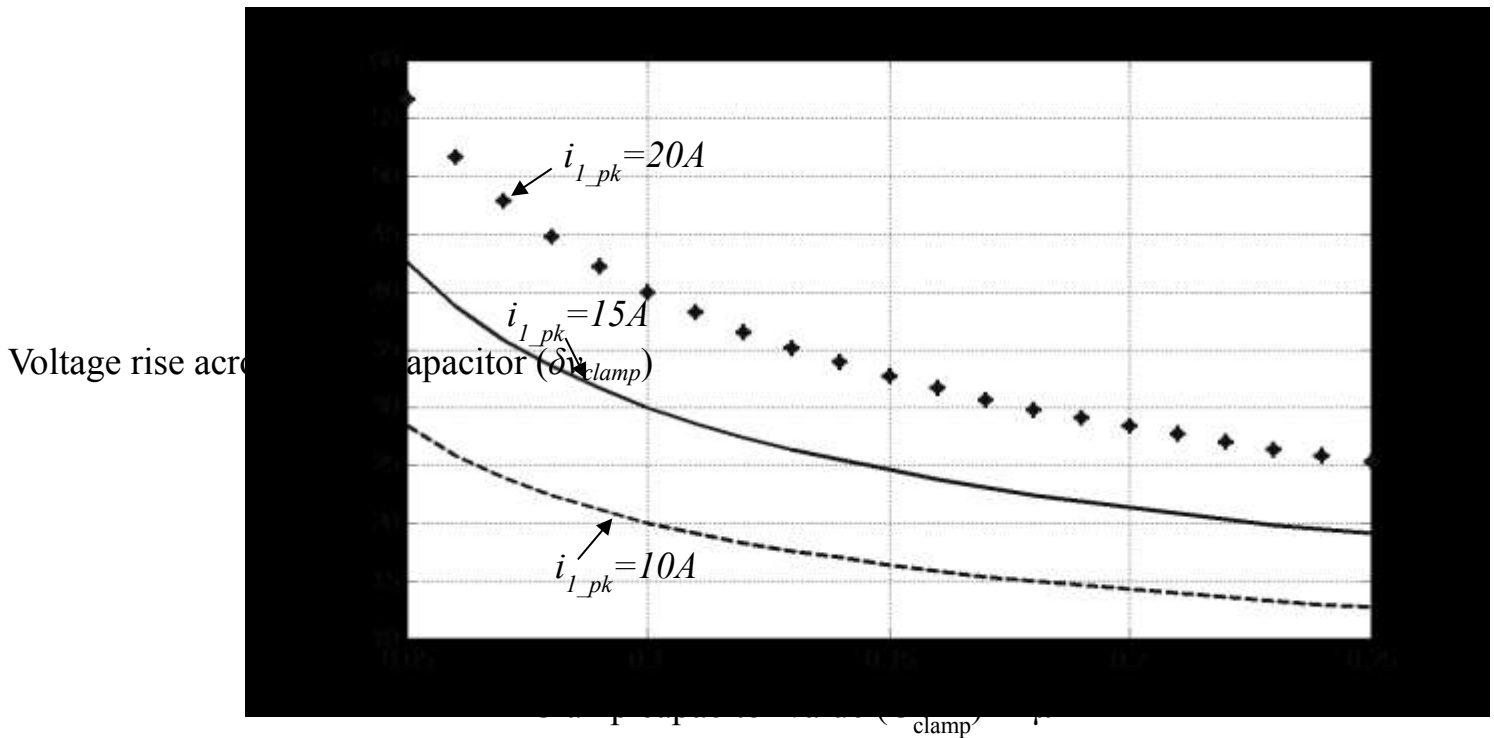
Figure 3-12 Peak voltage rise across clamp capacitor for different capacitor values.

3.3.4   Frequency range selection

A frequency range needs to be selected so that the converter operates in ZVS within that selected range. As the operating frequency of the converter is increased, frequency dependent losses such as switching losses also increase. If the converter's switching frequency is too low, then the size of the transformer and output capacitor need to be increased.

Based on equation (3.34), the variation in frequency need to accommodate the resonant mode can be estimated and this is given in Figure 3-14. From Figure 3-11 it can be understood even with frequency variation, beyond 2.2 ms to 6.1 ms for a 60Hz half cycle, ZVS will be missed. From the graph in Figure 3-13 the estimated frequency for this range
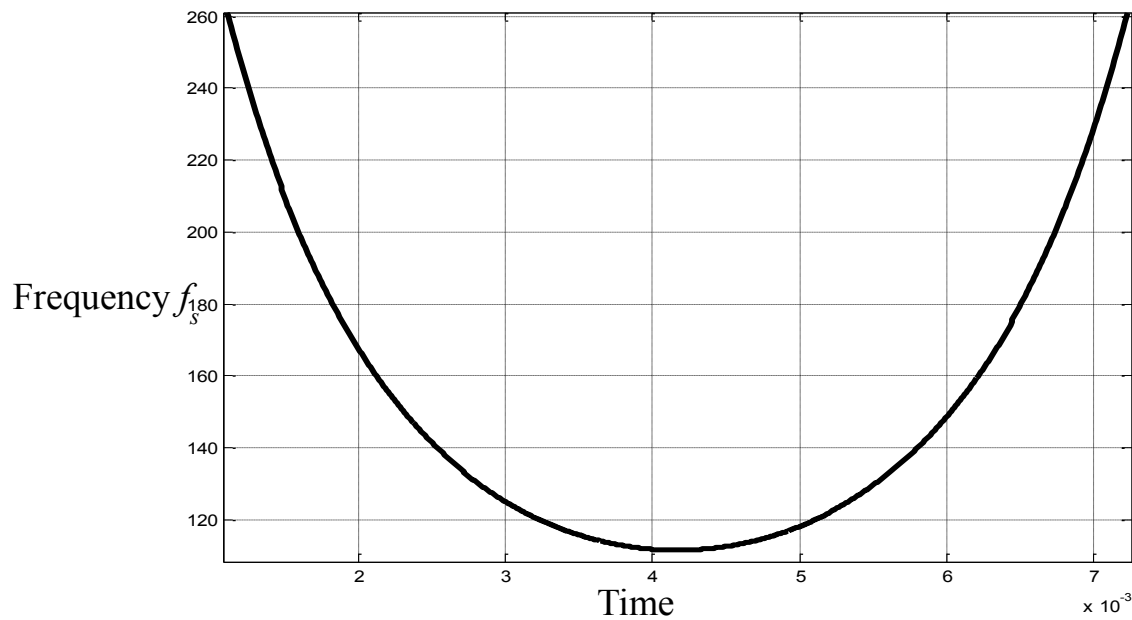
Figure 3-13 Frequency variation.

is around 110 kHz to 170 kHz. Therefore, based on Figure 3-13 and Figure 3-11 and allowing a bit more flexibility the frequency limits are chosen as 80 kHz-to 200 kHz.

3.4 Simulation results

The proposed flyback micro-inverter was simulated using PSIM software. The converter was simulated with the same specifications that were given in the previous section and with the following component values: L_m=12.8µH, C_{clamp}=0.12µF, N=0.4,N_{tr}=7.8.

In Figure 3-14, it is shown that the gate pulse on the voltage across the switch v_{ds} reaches zero before the switch is turned on so that ZVS is achieved. In Figure 3-15 switch current i_1 is shown with the gating pulses. It can be seen that the current through the switch goes negative before it is turned on, which shows that the anti-parallel diode of the switch

conducts and a ZVS turn-on is achieved. Figure 3-17 shows that the converter is operated with constant frequency, at the lowest selected switching frequency, as the duty cycle becomes very small so that it operates like the converter presented in the previous chapter. In Figure 3-18 the complete AC cycle for the primary current and the output load current is shown. It can be seen from the primary current waveform that there are negative current portions during most of the AC cycle so that a ZVS turn-on can be achieved.
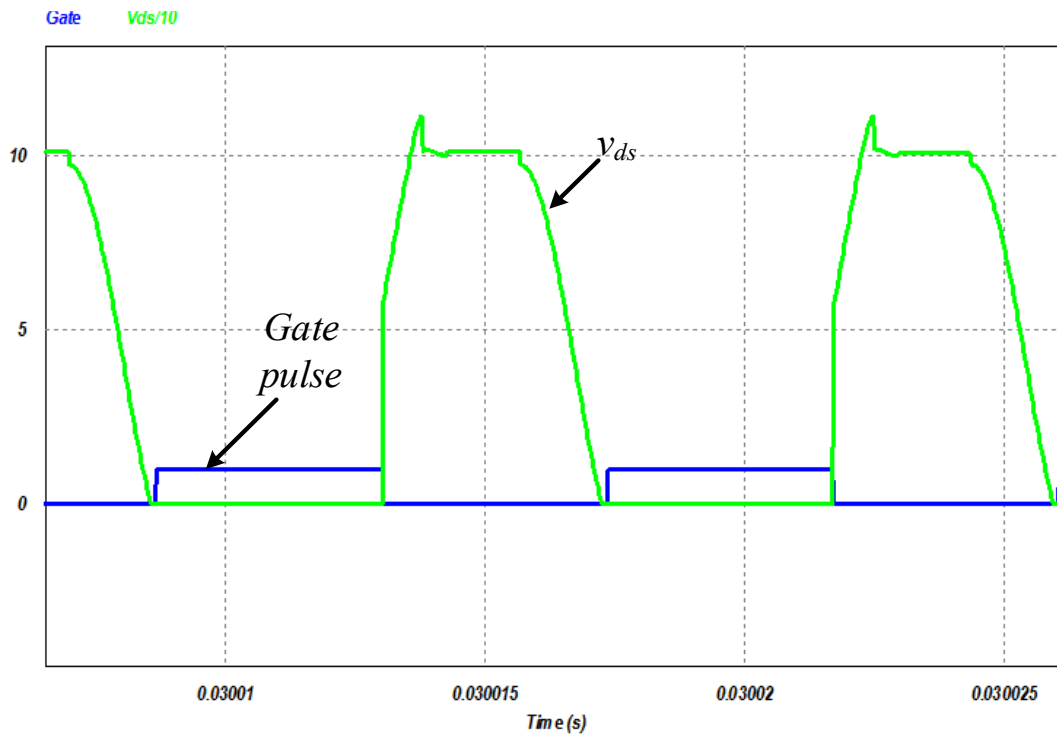
Figure 3-14 Voltage across switch S₁ and gate pulse.
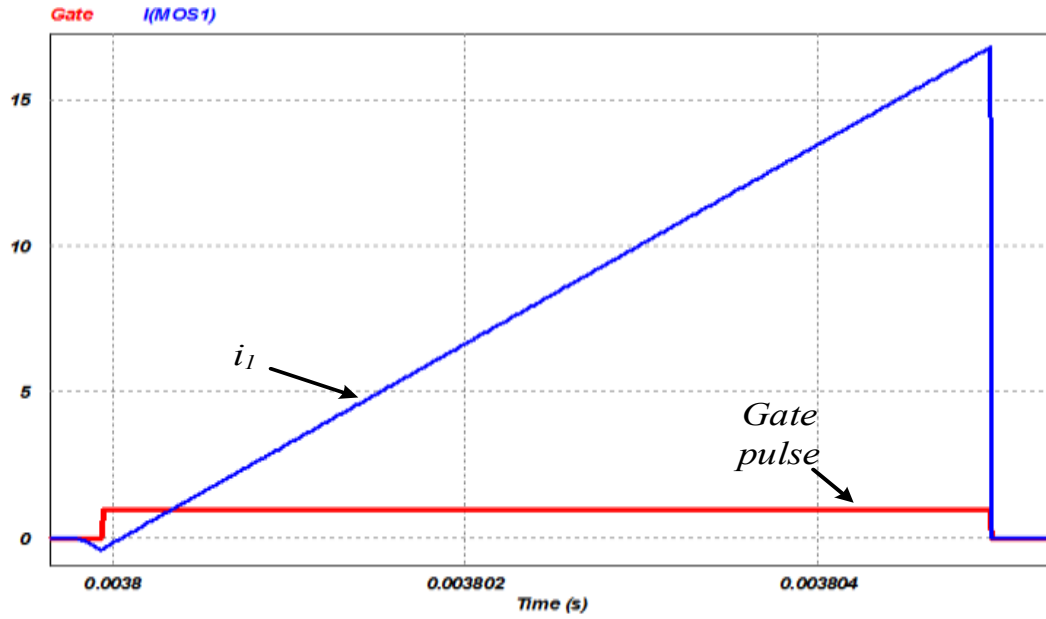
Figure 3-15 Switch current and gate pulse.
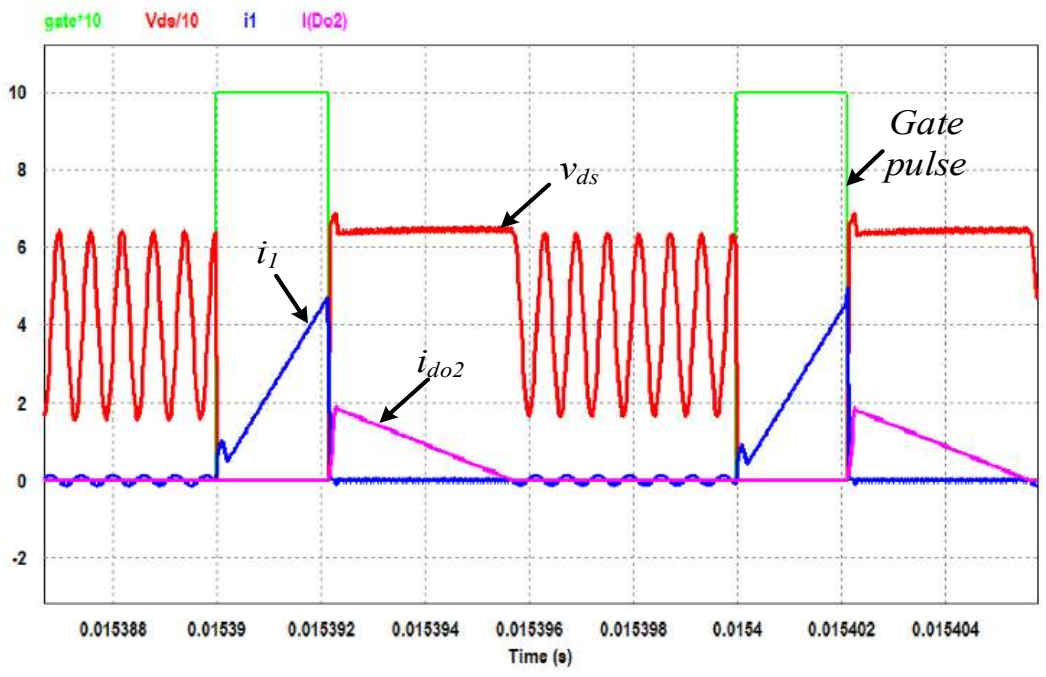
Figure 3-16 waveforms during small duty cycle.
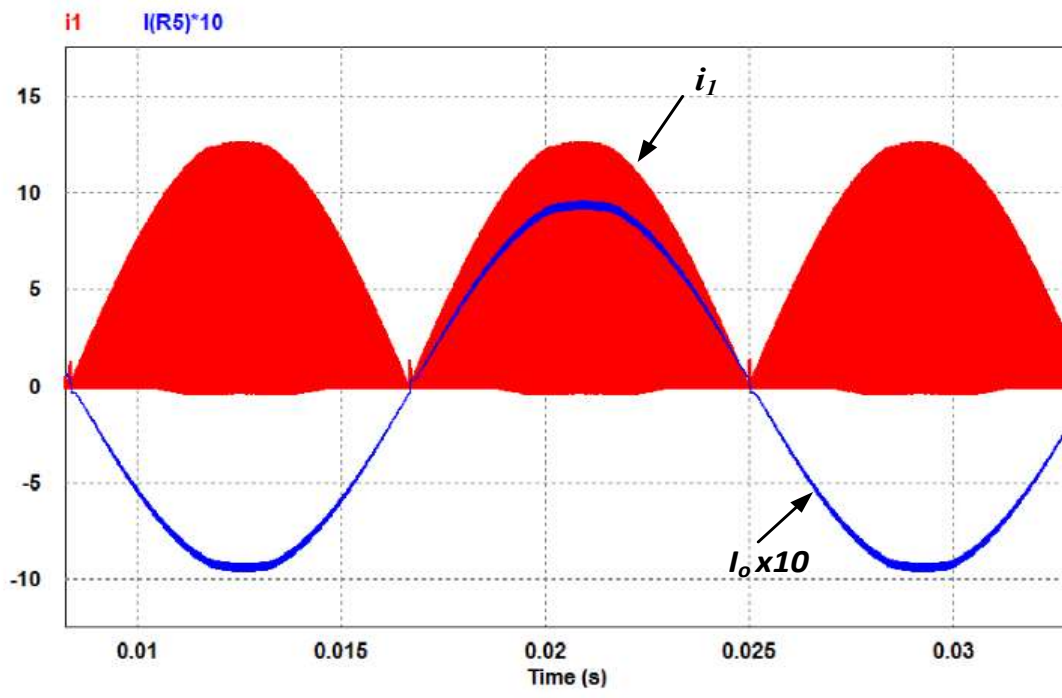
Figure 3-17 Load current and switch current.

3.5 Experimental results

A 110VAC grid connected inverter was built according to the following specifications: input voltage V_{in} = *45VDC*, maximum output power $P_{o,max}$ = *100W* and switching frequency range *80 kHz < f_{sw} < 200 kHz*. The same component values were used in the experimental prototype as were used in the simulations. A TMS320f28335 DSP was used to generate the gating pulses for the primary and the secondary switches.

The current through S_1 and the voltage across it are shown in Figure. 3-18. It can be seen that the switch is turned on while current is flowing through its body diode (negative current) so that it can be turned on with ZVS. In Figure 3-19, the switch voltage, and the snubber current are shown. It can be seen from Figure 3-20 that the converter does produce an AC output voltage.
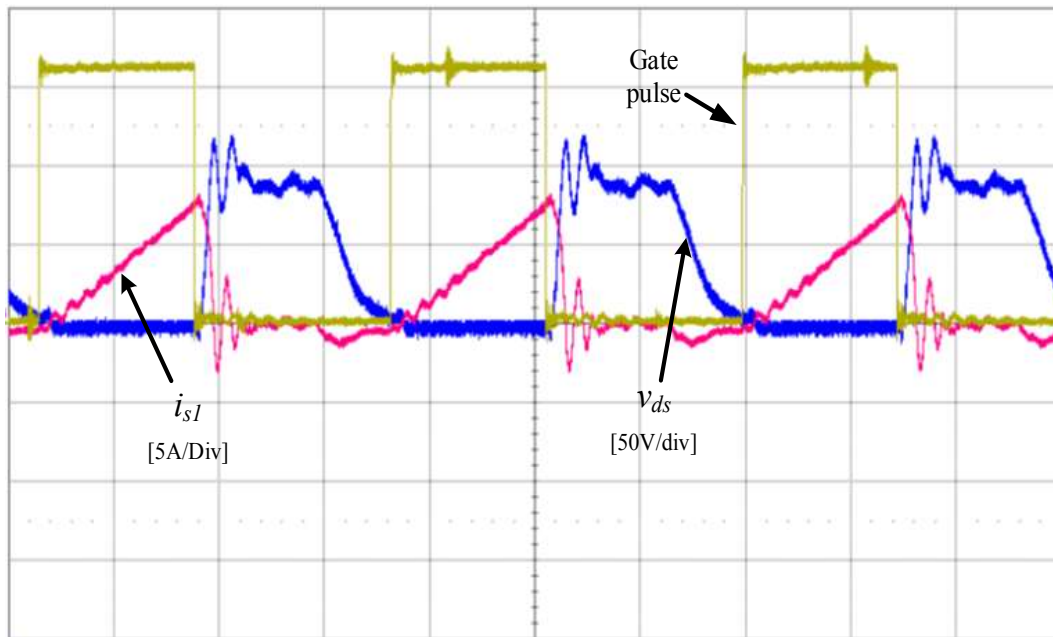
Figure 3-18 Primary current, voltage across S_1 and gate pulse.
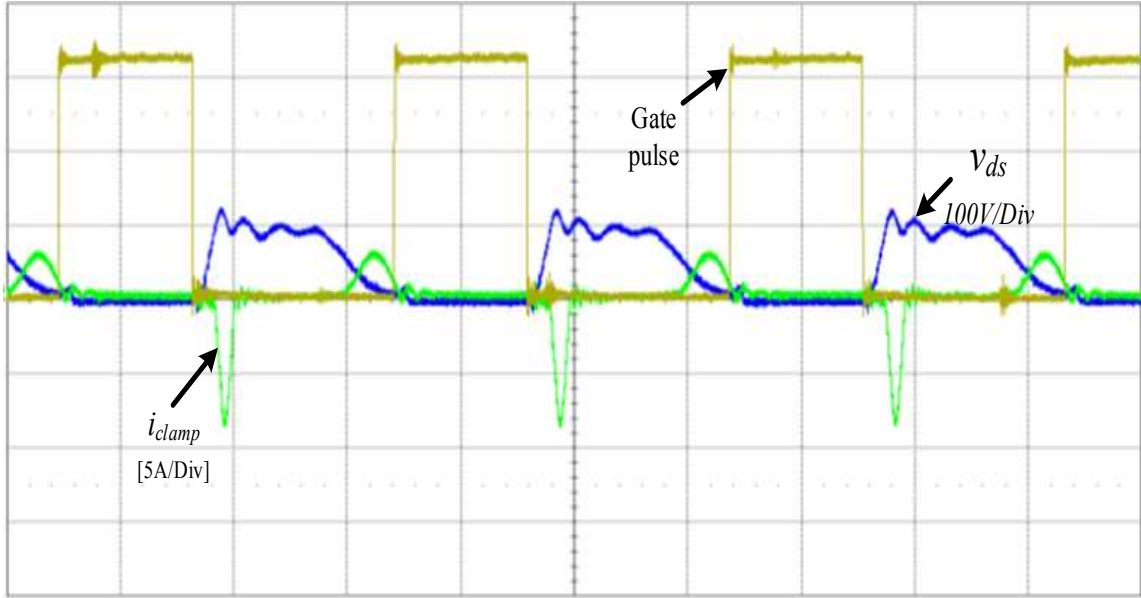
Figure 3-19 Voltage across S₁, clamp capacitor current and gate pulse.
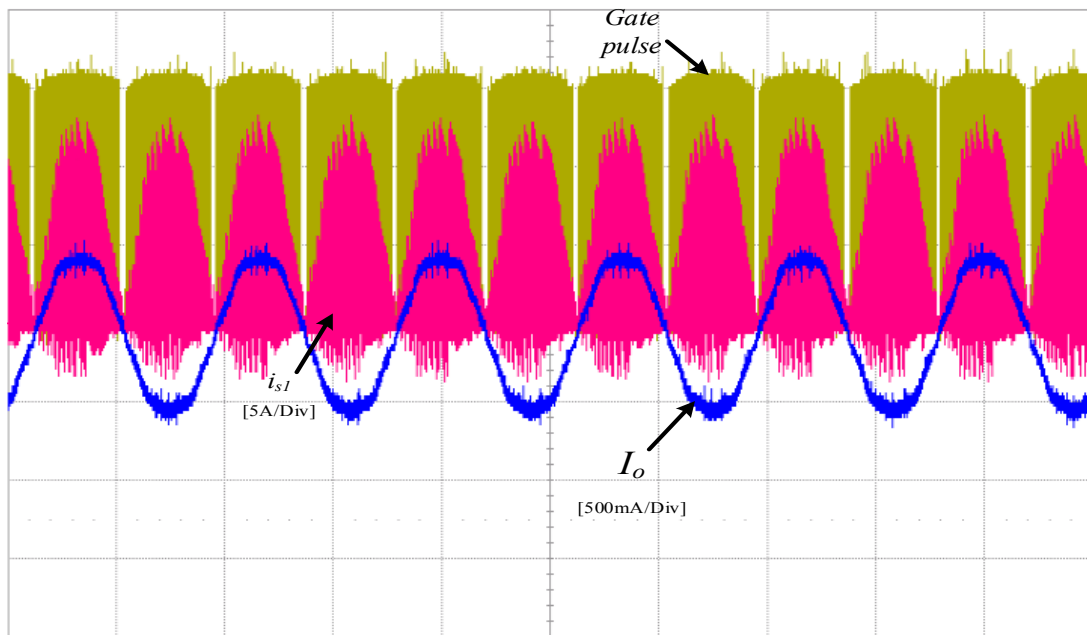
Figure 3-20 Load current, regenerative current, switch current and gate pulses.

A graph of converter efficiency vs load comparison for the cases when the converter is implemented with the ZVS passive snubber and with an active clamp is shown in Fig. 5. The active clamp implementation was a standard implementation and was used as a benchmark. The active clamp converter was also build with the same specification as the proposed converter and it was switched at 100 kHz of switching frequency. It can be seen that a maximum gain in efficiency of more than 1% can be achieved by using the cheaper passive snubber instead of the active snubber. From the efficiency graph it can be seen that at light load conditions the active clamp converter is more efficient than the proposed ZVS converter, as at light load the ZVS range throughout the AC cycle is reduced for the proposed converter. As the load crosses 60W load level, it was found that the proposed converter is more efficient than the active clamp converter.
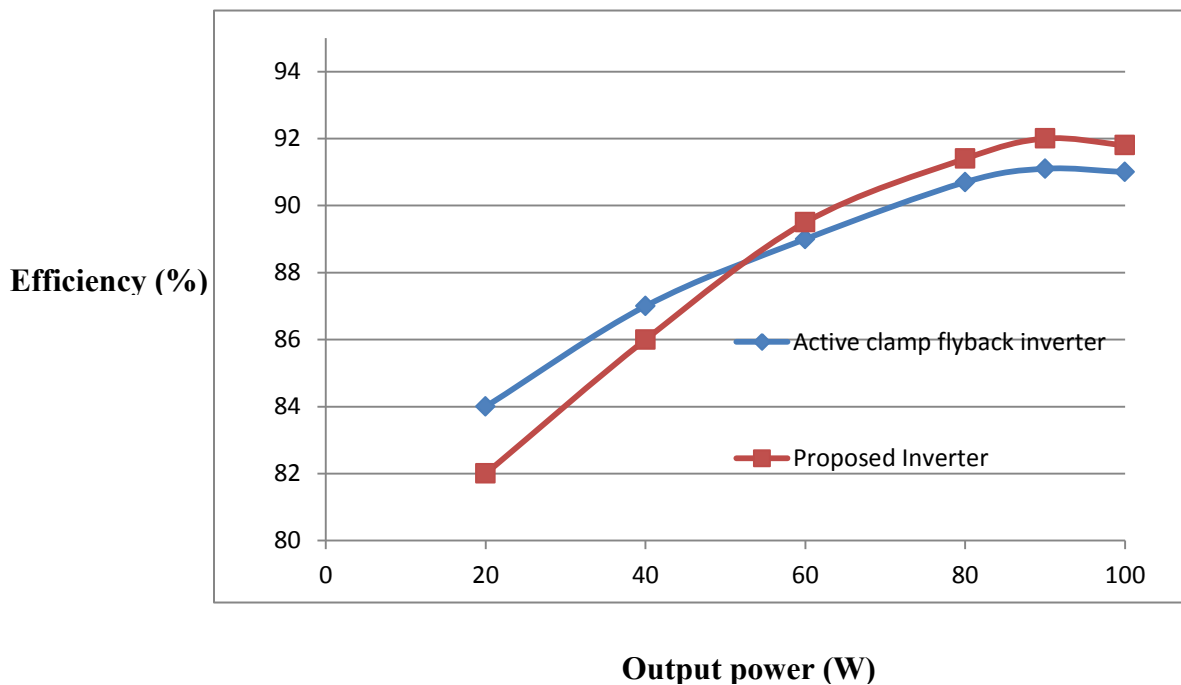
Figure 3-21 Efficiency comparison.

3.6   Summary

A novel technique for improving the efficiency of a basic dc-ac flyback micro-inverter was proposed in this chapter. The proposed efficiency improving technique was based on a simple snubber, consisting of just a few passive elements and the use of a variable switching frequency technique that is based on quasi-resonant converter principles to achieve ZVS. The new flyback micro-inverter was presented, its modes of operation of the converter were discussed and analyzed and the design of the converter was demonstrated with an example. Simulation and experimental results obtained from a lab prototype confirmed the feasibility of the proposed converter.

Chapter 4

4   Conclusion

In this chapter, the contents of the thesis are summarized, conclusions resulting from the thesis work are presented, the contributions of the thesis to the power electronics literature are stated, and suggestions for future work are given.

4.1   Summary

Renewable energy systems have been popular in recent years due to their promise of unlimited energy and due to environmental concerns about other, less clean, forms of energy. Solar energy systems are especially attractive and considerable research has been done on such systems. An important part of any solar energy system are the DC-AC converters (inverters) that convert DC power into AC power that can be fed to the grid. There are three basic types of inverter architectures, each with their merits and demerits. These architectures are central inverters, string inverters and micro-inverters. The focus of this thesis has been on micro-inverters.

Micro-inverters are small DC-AC converters that are attached to each solar photovoltaic (PV) panel of a solar energy system. The main advantage of using micro-inverters is that they make the solar energy system less prone to the effects of shading. They are typical low power converters (100 W- 200W) that are based on low power DC-DC converter topologies. Many micro-inverters are based on the DC-DC flyback converter as this converter is the simplest DC-DC converter with transformer isolation. A transformer is

needed to step up the voltage that is obtained from the PV panels so that it can match the level needed to be fed to the grid.

The main objective of this thesis has been to improve the efficiency of the conventional DC-AC flyback micro-inverter. Two approaches to doing this were studied. The first involved the addition of a simple regenerative snubber to the main topology so that the turn-off losses of the primary switch can be reduced. The main advantages of this snubber are that energy fed to the snubber can be fed to the output and that the snubber itself is very simple, consisting of just a few passive components and an auxiliary winding taken from the main transformer. The second approach was to operate this new converter with a variable switching frequency technique that allows the primary switch to operate with zero-voltage switching (ZVS) so that the primary switch turn-on losses can be reduced as well as the turn-off losses.

The operation of both converters was explained in detail in the thesis, the design of both approaches was discussed and the effectiveness of the two proposed approaches was confirmed with experimental results obtained from prototype converters. In the first case, it was shown the converter with the regenerative energy snubber is more efficient than the same converter with a conventional resistor-capacitor-diode (RCD) snubber, which is the simplest and cheapest and most widely used passive snubber. In the second case, it was shown the converter with the regenerative snubber and the ZVS technique is more efficient and the active clamp flyback micro-inverter, which was used as a benchmark as it is the most popular ZVS method for flyback converters.

4.2 Conclusions

The following conclusions can be made based on the work performed in this thesis:

i. Implementing a flyback micro-inverter with a regenerative snubber makes it significantly more efficient (more than 5%) than a flyback micro-inverter with a passive RCD snubber.

ii. Implementing a flyback micro-inverter with a regenerative snubber and the variable switching quasi-resonant ZVS technique makes it more efficient (more than 1%) than an active clamp ZVS flyback micro-inverter.

4.3 Contributions

The main contribution of this thesis to the power electronics literature is that two new flyback micro-inverter implementations were proposed and their feasibility was confirmed with simulation and experimental work.

4.4 Future Work

For future work, the proposed flyback micro-inverter implementations can be implemented in higher power topologies. The maximum power level used for this work was 100 W, which is a typical power level for flyback micro-inverters. Research can be performed to see if the flyback micro-inverters proposed in this thesis can be adapted for higher power levels by making modifications such as paralleling multiple flyback micro-inverters or by changing the topology so that it has a three-phase DC input.

5 Reference

[1]   EPIA; Global market outlook for Photovoltaics, Report 2013-2017.

[2]   German Advisory Council on Global Change, WBGU Berlin; www.wbgu.de; Renewable Energy Policy Network for the 21st Century, Renewables, Global Status Report 2006.

[3]   S. B. Kjaer, J. K. Pedersen and F. Blaabjerg, "A review of single-phase grid-connected inverters for photovoltaic modules," *IEEE Trans. on, Ind. Appl.,* vol. 41, pp. 1292-1306, 2005.

[4]   Q. Li and P. Wolfs, "A Review of the Single Phase Photovoltaic Module Integrated Converter Topologies With Three Different DC Link Configurations," *IEEE Trans. on Power electron.* vol. 23, pp. 1320-1333, May 2008.

[5]   M. Calais, J. Myrzik, T. Spooner and V. G. Agelidis, "Inverters for single-phase grid connected photovoltaic systems-an overview,"in *proc. IEEE PESC,* 2002, pp. 1995-2000.

[6]   R. H. Wills, S. Krauthamer, A. Bulawka and J. P. Posbic, "The AC photovoltaic module concept," in *Proc. IEEE IECEC, 1997*, pp. 1562-1563 vol.3.

[7]   R. C. Variath, M. A. E. Andersen, O. N. Nielsen and A. Hyldgard, "A review of module inverter topologies suitable for photovoltaic systems," in *Proc. IEEE IPEC, 2010*, pp. 310-316.

[8]   F. Edwin, X. Weidong and V Khadkikar, "Topology review of single phase grid-connected module integrated converters for PV applications," in *Proc. IEEE IECON, 2012*, pp.821-827.

[9]   A.C. Kyritsis, E.C. Tatakis, and N.P. Papanikolaou, "Optimum design of the current-source flyback inverter for decentralized grid-connected photovoltaic systems," *IEEE Trans. Energy Conv.,* vol. 23, no.1, pp. 281-293, Mar. 2008.

[10]   A.C. Kyritsis, E.C. Tatakis, and N.P. Papanikolaou, "A Weighted-Efficiency-Oriented Design Methodology of Flyback Inverter for AC Photovoltaic Modules," *IEEE Trans. on Power electron,* vol.27, no.7, pp.3221-3233, July 2012

[11]   X. Cao and W. Zhang, "Grid-connected solar Micro-inverter reference design," in *Proc. IEEE ICAE,* pp.239-243.

[12]   L. Yanlin and R.Oruganti, "A low cost flyback CCM inverter for AC module application," *IEEE Trans. Power electron.* vol. 27, no. 3, pp. 1295-1303, Mar. 2012.

[13]   T. V. Thang, N.M. Thao, D.H. Kim and J.H. Park, "Analysis and design of a single-phase Flyback microinverter on CCM operation," in *Proc. IEEE IPEMC, 2012,* pp.1229-1234.

[14]   N. Kasa, T. Iida, and A.K.S. Bhat, "Zero-voltage transition flyback inverter for small scale photovoltaic power system," in *Proc. IEEE PESC,* 2005, pp. 2098-2103.

[15]   Q. Mo, M. Chen, Z. Zhang, M. Gao and Z. Qia, "Research on a non-complementary active clamp flyback converter with unfolding DC-AC inverter for decentralized grid-connected PV systems," in *Proc. IEEE Ener. Conv. Cong. & Expo. (ECCE)*, 2011, pp 2481-2487.

[16]   J.K. Park; Y.H. Kim; Y.H. Ji; Y.C. Jung and C.Y. Won, "A novel control strategy of an active clamped flyback inverter with synchronous rectifier for a photovoltaic AC module system," in *Proc. IEEE ICPE & ECCE, 2011*, pp.401-405.

[17]   J.S. Kang, Y.H. Kim, S.J.Youn, C.Y.Won and Y.C. Jung, "Active clamp flyback inverter considering leakage inductance of transformer for photovoltaic AC modules," in *Proc. IEEE VPPC,2012,* pp.1379-1383.

[18]   Y.H. Kim, J.G. Kim, Y.H. Ji, C.Y. Won and T.W. Lee, "A new control strategy of active clamped flyback inverter for a photovoltaic AC module system," *in Proc. IEEE ICPE & ECCE, 2011,* pp.1880,1885.

[19]   N. Sukesh, M. Pahlevaninezhad and P. Jain, "Analysis and Implementation of a Single Stage Flyback PV-Micro Inverter with Soft Switching," *IEEE Trans. on Ind.Elec.*, vol.PP, no.99, pp.1,1, 0

[20]   S. Chandhaket, K. Ogura, M. Nakaoka and Y. Konishi, "High-frequency flyback transformer linked utility-connected sinewave soft-switching power conditioner using a switched capacitor snubber," *Proc. Int. Power Elec. and Motion Cont. Conf. (IPEMC)* 2004, pp. 1242-1247 .

[21]   Q. Mo, M. Chen, Z. Zhang, Y. Zhang and Z. Qian, "Digitally controlled active clamp interleaved flyback converters for improving efficiency in photovoltaic grid-connected micro-inverter," in *Proc. IEEE Appl. Power Elec. Conf. (APEC) 2012.*, pp.555-562.

[22]   Z. Zhang, X.F. He and Y.F, Liu, "An Optimal Control Method for Photovoltaic Grid-Tied-Interleaved Flyback Microinverters to Achieve High Efficiency in Wide Load Range," *IEEE Trans. on Power electron,* vol.28, no.11, pp.5074-5087, Nov. 2013

[23]   G.J. Yin, W.H. Fei; C.G.Cheng and Y. Xing, "Research on photovoltaic grid-connected inverter based on soft-switching interleaved flyback converter," in *Proc. IEEE ICIEA, 2010*, pp.1209-1214.

[24]   M. Gao, M. Chen, Q. Mo, Z. Qian and Y. Luo, "Research on output current of interleaved-flyback in boundary conduction mode for photovoltaic AC module application," in *Proc. IEEE Ener. Conv. Cong. & Expo. (ECCE), 2011*, pp.770-775.

[25]   F.F. Edwin, W. Xiao and V. Khadkikar, "Dynamic Modeling and Control of Interleaved Flyback Module Integrated Converter for PV Power Applications," *IEEE Trans. on, Ind. Appli.,* vol.PP, no.99, pp.1,1,April 2013.

[26]   Z. Zhang, X.F. He and Y.F. Liu, "An Optimal Control Method for Photovoltaic Grid-Tied-Interleaved Flyback Microinverters to Achieve High Efficiency in Wide Load Range," *IEEE Trans. on Power electron*, vol.28, no.11, pp.5074-5087, Nov. 2013

[27]   Y. Kanazawa and M. Yamamoto, "A novel compact single phase inverter using transformer-linked interleaved flyback converter," in *Proc. IEEE ICRERA, 2012,* pp.1,3.

[28]   Y. Kim, Y.Ji, J.G. Kim, Y. Jung and C.Y.Won, "A New Control Strategy for Improving Weighted Efficiency in Photovoltaic AC Module-Type Interleaved Flyback Inverters," *IEEE Trans. on Power electron*, vol.28, no.6, pp.2688-2699, June 2013

[29]   Z. Zhang, X.F. He. X. Ren, X. Li and Y.F. Liu, "Multi-mode control for photovoltaic grid-connected interleaved flyback micro-inverters to achieve high efficiency in wide load range," in *Proc. IEEE Ener. Conv. Cong. & Expo. (ECCE)*, *2012,* pp.2433- 2438.

[30]   J.W. Jang, Y.H. Kim, D.K. Ryu, C.Y. Won and Y.C. Jung, "High efficiency control method for interleaved flyback inverter with synchronous rectifier based on photovoltaic AC modules," in *Proc. IEEE IECON 2012*, pp.5720-5725.

[31]   S. Jain and V. Agarwal, "A Single-Stage Grid Connected Inverter Topology for Solar PV Systems With Maximum Power Point Tracking," *IEEE Trans. on Power electron*,vol. 22, pp. 1928-1940, Sept., 2007.

[32]   E.S. Sreeraj, K. Chatterjee and S. Bandyopadhyay; , "One-Cycle-Controlled Single-Stage Single-Phase Voltage-Sensorless Grid-Connected PV System," *IEEE Trans. on, Ind. Appl.,* vol.60, no.3, pp.1216-1224, Mar., 2013.

[33]   A. Chen, S. Daming, D. Chunshui and C. Zhang, "High-frequency DC link flyback single phase inverter for grid-connected photovoltaic system," in *Proc. IEEE PEDG, 2010*, pp. 364-367.

[34]   N. Kasa, T. Iida and L. Chen, "Flyback Inverter Controlled by Sensorless Current MPPT for Photovoltaic Power System," *IEEE Trans. on, Ind. Appl.*vol. 52, pp. 1145-1152, Aug., 2005.

[35]   Y. Chen and K. M. Smedley, "A cost-effective single-stage inverter with maximum power point tracking," *IEEE Trans. on Power electron*, vol. 19, pp. 1289-1294, Sept., 2004.

[36]   A. Abramovitz, S.L. Chih, and K. Smedley, "State-Plane Analysis of Regenerative Snubber for Flyback Converters," *IEEE Trans. on Power electron.*, vol.28, no.11, pp.5323-5332, Nov., 2013

[37]   J.D. Sperb, I.X. Zanatta, L. Michels, C. Rech, and M. Mezaroba, "Regenerative Undeland Snubber Using a ZVS PWM DC–DC Auxiliary Converter Applied to Three-Phase Voltage-Fed Inverters," *IEEE Trans. Ind. Electron.*, vol.58, no.8, pp.3298-3307, Aug., 2011

[38]   J. Bauman and M. Kazerani, "A Novel Capacitor-Switched Regenerative Snubber for DC/DC Boost Converters," *IEEE Trans. Ind. Electron.*, vol.58, no.2, pp.514-523, Feb., 2011

[39]   T.H. Ai. "A novel integrated non-dissipative snubber for flyback converter," in *Proc. IEEE ICSS,* 2005, pp. 66 - 71.

[40]   Y. Konishi and Y.F. Huang, "Soft-switching buck boost converter using pulse current regenerative resonant snubber," *IET Electronics Letters* , vol.43, no.2, pp.127-128, Jan., 2007

[41]   P. Fleury and K. A. Haddad, "Universal input voltage, unity power factor, high efficiency flyback rectifier with regenerative snubber," in *Proc. IEEE, CCECE,2005*, pp.595-598.

[42]   A. Abramovitz, T. Cheng and K. Smedley, "Analysis and Design of Forward Converter With Energy Regenerative Snubber," *IEEE Trans. on Power electron.*, vol.25, no.3, pp.667-676, Mar., 2010

[43]   A. Matsushita, H. Tai; I. Yasuoka and T. Matsumoto, "Inverter circuit with the regenerative passive snubber," in *Proc. IEEE PCC, 2007* , pp.167-171.

[44]   G.C. Huang, T.J. Liang and K.H. Chen, "Losses analysis and low standby losses quasi-resonant flyback converter design," in *Proc. IEEE ISCAS, 2012*, pp.217-220.

[45]   M.T. Zhang, M.M. Jovanovic and F.C.Y. Lee, "Design considerations and performance evaluations of synchronous rectification in flyback converters," *IEEE Trans. on Power electron.*, vol.13, no.3, pp.538-546, May, 1998

[46]   W.A.Tabisz; P.M. Gradzki and F.C.Y. Lee, "Zero-voltage-switched quasi-resonant buck and flyback converters-experimental results at 10 MHz," *IEEE Trans. on Power electron.*, vol.4, no.2, pp.194-204, April, 1989

[47]   R. Watson, F.C.Y. Lee and G.C. Hua, "Utilization of an active-clamp circuit to achieve soft switching in flyback converters," *IEEE Trans. on Power electron.*, vol.11, no.1, pp.162-169, Jan., 1996

[48]   K.H. Liu and F.C.Y. Lee, "Zero-voltage switching technique in DC/DC converters," *IEEE Trans. on Power electron.*, vol.5, no.3, pp.293-304, July, 1990

[49]   M.M. Jovanovic, D.C.Hopkins and F.C.Y. Lee, "Evaluation and design of megahertz-frequency off-line zero-current-switched quasi-resonant converters," *IEEE Trans. on Power electron.*, vol.4, no.1, pp.136-146, Jan., 1989

[50]   R.B. Ridley, W.A. Tabisz, F.C.Y. Lee and V Vorperian, "Multi-loop control for quasi-resonant converters," *IEEE Trans. on Power electron.*, vol.6, no.1, pp.28-38, Jan., 1991

[51]   C.S. Lin; "Summation of finite series of integers ," *Canadian Mathematical Society*, pp510,513, 2010.

Curriculum Vitae

Name: Aniruddha Mukherjee

Post-secondary   West Bengal University of technology
Education and   Kolkata, West Bengal, India.
Degrees: 2005-2009 B.Tech.

                      The University of Western Ontario
                      London, Ontario, Canada
                      2011-2013 M.E.Sc

Honours and   Western University Graduate Scholarship
Awards: Outstanding Technical Presentation Award, APEC, 2013.

Related Work   Teaching Assistant, Research Assistant
Experience   The University of Western Ontario
                      2011-2013

Publications:

"Passive Snubber Circuit for Flyback Microinverters in Solar Energy Systems" *IEEE Applied Power Electronics Conference (APEC)* 2013, Long Beach CA.

"Flyback Quasi-resonant inverter with Variable Frequency Controlled ZVS" *IEEE Energy Conversion Congress & Expo (ECCE)* 2013, Denver CO.

"Comparative Analysis of Flyback Inverters for Solar Energy Systems" *IEEE International Telecommunication Energy Conference (INTLEC)* 2013, Hamburg, Germany.